WRINKLES

USE OF WRINKLES FOR FABRICATION
OF
STRETCHABLE ELECTRODES AND OMNIPHOBIC SURFACES

By

YUTING CHAN, B.Eng., B.A.

A Thesis Submitted to the School of Graduate Studies
in Partial Fulfilment of the Requirements
for the Degree Master of Applied Science

McMaster University

MASTER OF APPLIED SCIENCE (2018)
(Engineering Physics)

MCMASTER UNIVERSITY
Hamilton, Ontario, Canada

TITLE:	Use of wrinkles for fabrication of stretchable electrodes and omniphobic surfaces
AUTHOR:	Yuting Chan, B.Eng., B.A.
SUPERVISOR:	Dr. Leyla Soleymani
NUMBER OF PAGES:	xviii, 110

Lay Abstract

Wrinkling is a phenomenon often seen in real life, such as on the skin of a dried plum or human. It is possible to fabricate such wrinkles through having a stiff thin film adhered to an elastic foundation and compressing the foundation. The wrinkles are useful for fabrication of stretchable electrodes as their structure allows the film to stretch without breaking through unfolding. Here, we fabricated stretchable electrodes by transferring such wrinkled structures onto elastic foundation. These stretchable electrodes are shown to be able to detect the concentration of glucose in solution even when stretched. These electrodes are important for creating wearable devices that can monitor glucose levels or other substance continuously. Wrinkles also work as part of hierarchical structure which are helpful for trapping air beneath droplets of fluids. Here we incorporate wrinkles with nanoparticles which helps to make surfaces repellent to both water and oil. Such a function is important for self-cleaning surfaces and can also be used for patterning of surfaces for selective deposition of fluid.

Abstract

The buckling of stiff film on a substrate had been of great interest as this response happen spontaneously and is self-organizing. This provides an unconventional, scalable and easy way to fabrication surfaces with tunable structures from the range of nanometers to micrometers. We optimized a process to fabricate stretchable electrodes by transferring wrinkled gold onto elastomer. We tested their electrochemical sensing functionality through detection of glucose concentration with or without strain. Results showed that the stretchable electrodes provide high sensitivity for the detection of glucose (860 ± 60 $\mu A/mM.cm^2$), comparable to electrodes before transfer. The current detected was also consistent under strain. Investigation of the resistance indicates that the electrode configuration under strain is important as current running parallel to direction of strain is much more affected under tension. We also developed a fast and facile process to fabricate surfaces that consisted of wrinkles and nanoparticles. Using such surfaces, we tested the omniphobicity effect of hierarchical structures consisting of wrinkles and nanoparticles. Results show that all the fluorinated structured surfaces were hydrophobic, ranging from water contact angle of 125° for wrinkled surfaces to 155° for hierarchical surfaces. The surfaces that were either wrinkled or decorated with nanoparticles were oleophilic with low hexadecane contact angles (~26° and ~55° respectively). The combination of both structures achieved oleophobicity of more than 110°. The effectiveness of nanoparticles for low surface tension liquid were due to its re-entrant like structure. The omniphobic surfaces

were also shown to be repellent to blood (>135°), making it a potential material for use medical devices.

Acknowledgements

I would like to express my gratitude to my supervisor, Dr. Leyla Soleymani for her support, ideas and constant excitement about my work. Without her enthusiasm, confidence and constant guidance, my research would not have been as interesting or proceeded as smoothly.

I would like to thank the staff of the Biointerfaces Institute, the Centre for Emerging Device Technologies and the Canadian Centre for Electron Microscopy for the use of their facilities and assistance with my work.

I would like to thank my lab-mates, Eric Daigle, Jie Yang, Sudip Saha, Larona Toteng and Amin Hosseini who were there from the start. To those people of the group, past and present, who could not be named here, it was a pleasure to have the opportunity to interact with such a great group of people. All of you have made this journey infinitely more enjoyable.

I would like to thank my parents for their constant support through all the unconventional decisions I have made in my life. To my brother and relatives, thank you for being there for the family when I was not able to.

Finally, to everyone who had contributed in any way to making this possible – thank you.

Table of Contents

List of Figures and Tables

Figures

Tables

List of all Abbreviations and Symbols

AFM: Atomic force microscopy.

Ag: Silver.

AgCl: Silver chloride.

Au: Gold.

AuNPs: Gold nanoparticles.

CA: Chronoamperometry.

CNT: Carbon nanotubes.

Cr: Chromium.

CV: Cyclic voltammetry.

PA-CVD: Plasma assisted chemical vapour deposition.

PAD: Pulsed amperometric detection.

PDDA: Polydiallyldimethylammonium chloride.

PDMS: Polydimethylsiloxane.

PET: Polyethylene terephthalate.

Ref: References.

S/n: Serial number.

SEM: Scanning electron microscope.

SiNPs: Silica nanoparticles.

TEM: Transmission electron microscopy.

Ti: Titanium.

TLC: Thin layer chromatography.

UVO: Ultraviolet-ozone.

α: Sliding angle.

θ: Contact angle.

θ_A: Advancing contact angle.

θ_R: Receding contact angle.

Declaration of Academic Achievement

The author is the first author and main contributor of the articles included in this thesis.

The detailed contributions of co-authors are detailed in the following preface section.

Preface

This is a sandwich thesis. The first paper consisted of contributions by Marta Skreta and Hannah McPhee, Sudip Saha and Ryan Deus who, with inputs from the author, assisted with: (a) refinement of the electrode transfer process initiated by the author, (b) collection of electrochemistry and resistivity data, and (c) providing written preliminary analysis of electrochemistry and resistivity data. Strain set up and surface characterisation was done by the author. Overall analysis and presentation of data was adjusted and revised by the author. Manuscript was written mainly by the author. Dr. Soleymani assisted with helpful suggestions and revision of the manuscript.

The second paper consisted of contributions from Sara Imani and Kenneth Rachwalski. Kenneth, with Sara, assisted with collection of data for bacteria adhesion. Sara assisted with collection of data for contact angle measurements for blood and adhesion for blood and bacteria. She also contributed in writing for the analysis of these data. The writing of the rest of the manuscript was done by the author. Dr. Soleymani assisted with helpful suggestions and revision of the manuscript.

Title: Stretchable wrinkled gold electrode for electrochemical sensing
Authors: Yuting Chan, Marta Skreta, Hannah McPhee, Sudip Saha, Ryan Deus, Leyla Soleymani
Publication: Submitted to Analyst (Royal Society of Chemistry), under revision

Title: Omniphobic surfaces with hierarchical structures incorporating wrinkles and nanoparticles

Authors:	Yuting Chan, Sara Imani, Kenneth Rachwalski, Eric Brown, Tohid F. Didar, Leyla Soleymani
Publication:	-

Chapter 1

Wrinkles

1.1 Introduction

Wrinkles, folds and creases can be seen commonly in daily life, on human skins, in the folds of flowers and earth terrains. They are the physical manifestation of responses to the elastic instabilities caused by strain in different systems. As these buckling responses are spontaneous and self-organizing, the creation of wrinkles, folds and creases are easily manufactured on surfaces [1–5].

With exploration into the field of nanomaterials/nanoscience, there have been an increase in comprehension of the unique physical impact of systems of such length scale. These systems are often referred to as the meso-scale systems where structures have dimensions larger than ~2-20 nm but smaller than ~1-50 μm [6,7]. With reduced sizes, there is an increase in specific interfacial effect and finite size effects and these effects can be used to control the optical, electrical and magnetic properties of systems [8]. Some examples of such effects are quantized excitation [9], single-electron tunneling [10] and near field optical behavior [11]. It had also been reported that nanoscopic surface areas caused by pores in electrodes increase currents associated with kinetic-controlled electrochemical events [12]. Hence, the fabrication of systems with structures of such sizes is of great interest in many different fields.

Many of the conventional fabrication techniques are capable of fabricating detailed structures. Even so, they have their limitations. Photolithography is a widely used technique that is scalable with high throughput. Ion beam lithography, while having better resolution than photolithography, is limited by its low throughput as a serial technique [6]. Both techniques also require various specialised equipment. The use of moulding, while cost-effective and high throughput, requires the initial purchase or fabrication of the mould. This makes most of the conventional techniques expensive or unsuitable for rapid prototyping.

Even though buckling responses are mostly limited to rippled and wrinkled structures, the ability to rapidly achieve features with sizes ranging from nanometers to micrometers [13–15] through a simple process has great potential as an unconventional fabrication technique in many fields. The importance of making use of such technique for rapid prototyping cannot be understated as it allows a new idea or a new product to be more efficiently introduced into the market through reduction of the time and cost required for testing.

The study of wrinkles was initially motivated by it being a response that was to be avoided in sandwich panels [16]. However, it was later found to be a useful phenomenon for formation of structures from nanometers to micrometers for numerous applications. In literature, wrinkling had been reported as a viable way to determine elastic moduli of thin films [17,18], to improve electrochemical sensing [19–21] and photovoltaic efficiency [22], to create surfaces that are hydrophobic [3,23–26] or has changeable wetting [27–30], stretchable electrodes [31–34], transistors [35] or photovoltaic [36], biointerfaces with alignment of cells [37] and many others. As shown, wrinkling had been studied and applied to various applications but there are still areas where studies have been lacking. This work will focus on two areas of applications, stretchable electrochemical sensing and omniphobicity.

1.2 Objective of thesis

Objective 1:

In these two areas, the first objective is to design and develop a rapid and cost-effective procedure to create wrinkles that are easily functionalised. To keep the processes cost-effective and compatible with rapid prototyping, the processes shall be done on bench-top without the use of expensive specialised instruments, shall not take more than a few days and reasonably scalable in that more than ten samples can be created in one go.

Objective 2:

The second objective is to assess the functionalized wrinkles' viability in the two areas of stretchable electrochemical sensing and omniphobicity by measuring their performance. For stretchable electrodes, there are several performance categories: sensitivity, linearity and robustness. For omniphobicity, there are several performance categories: contact angle, sliding angle and robustness. In this work, robustness will not be examined.

Objective 3:

The third and final objective is to look at the feasibility of the devices created through the processes for more applications through tests for specific type of stretchable electrochemical sensing and omniphobicity.

1.3 Motivation

Both stretchable electrochemical sensing and omniphobicity were chosen for the studies as they are areas where their applications are in high demand and in-depth studies could provide useful improved insights.

1.3.1 Stretchable electrode for glucose detection

Diabetes is a chronic disease which had reached epidemic proportions [38]. Continuous glucose monitoring has been used for type 1 diabetes by an invasive device, an indwelling catheter inserted into the subcutis [38]. The creation of a less invasive glucose monitoring device, or of any other less invasive monitoring device, is paramount to the patient's quality of life. Other than electrochemical sensing through blood, it had been reported that sweat glucose is correlated to blood glucose level [39], which provides another pathway for glucose or other chemical monitoring through the patient's perspiration.

To achieve these, an electrode needs to conform to the surface of the skin [40], a property fundamental to stretchable materials. Stretchable electrodes had been developed either through the modifying the materials' intrinsic property or the materials' extrinsic structure [41,42]. One major method of using intrinsic property is by embedding conductive components into stretchable medium (S/n 1 to 4 of Table 1.1). In general, such a strategy has a major drawback where the conductivity decreases with applied strain [41]. Their performance can be improved in combination with modification of the materials' extrinsic structure using geometries such as wrinkles, coils, sponges and meshes (S/n 5 to 8 of Table 1.1). As shown in the tabulated data, extrinsic structures are more effective in increasing the performance of material at high strain. Specifically, wrinkled structure had exceptionally high performance of up to 400% strain as it allow unfolding under stretching, minimizing breaks and maintaining conductivity even at high strain.

Table 1.1: Examples of stretchable materials and the approximate strain they can withstand.

S/n	Description	Withstands	Ref
1	Silver and platinum nanoparticles on reduced grapheme oxide sheets embedded into nitrile butadiene rubber.	35% strain	43
2	Silver nanowires screen printed on substrate and embedded onto polydimethylsiloxane (PDMS) film.	50% strain	44
3	Ion gel printed on graphene and transferred onto rubber substrate.	5% strain	45
4	Carbon nanotube with silver nanoparticles were soaked into sponges.	90% strain	46
5	Reduced graphene oxide coated onto expanded polyacrylic ester substrate which is then cooled, forming wrinkles.	400% strain	47
6	Boron-doped silicon nanowire coils formed by buckling on ultraviolet-ozone (UVO) treated pre-strained PDMS substrate.	104% strain	48
7	Coating of metal thin film onto functionalized porous polyurethane sponges which is also filled with PDMS.	100% strain	49
8	Graphene grown through chemical vapour deposition onto copper mesh and copper removed. Mesh was then transferred onto PDMS substrate.	5% strain	50

There had been several stretchable electrodes proposed for glucose sensing (Table 1.1). As seen, only one of the detection methods is non-enzymatic. There are advantages in using non-enzymatic sensors [51]: stability (enzymes are affected by temperature, pH and humidity), simplicity (enzyme immobilization involves complex and reproducibility issues) and no limitation from oxygen (lack of oxygen negatively affect most enzyme electrodes). Some issues of non-enzymatic sensors are [51]: low current/sensitivity through glucose oxidation due to slow kinetics and interference of signals from adsorptive species on electrode.

As the electrooxidation of glucose is a kinetically controlled electrochemical events [52], nanoscopic surface areas due to wrinkles can help to increase currents detection. Wrinkles had already been shown to increase both electrochemical signal [21] and analytical sensitivity [19,53] with 2.93 increase of non-enzymatic glucose detection sensitivity for wrinkled gold compared to flat gold surfaces [53]. The interference of signal were also overcome through cleaning steps using pulsed amperometry detection [53].

These indicated that wrinkled gold electrode will work well as a stretchable electrode for electrochemical sensing. Hence, it is valuable to determine how well wrinkled electrodes work for electrochemical sensing under strain.

Table 1.2: Summary of stretchable electrodes tested for detection of glucose concentration.

Description	**Fabrication**	**Strain**	**Solution**	**Method**	**Sensitivity**	**Range (mM)**	**Ref**
Au/Cr and chlorinated silver electrodes with parylene insulating layer on PET	Photolithography, electron beam evaporation/disposition, acetone lift-off, oxygen plasma etching	-	Neutral	CA Enzymatic	2.3 µA/mM	0.05-0.2	[54]
CNT on patterned gold nanosheets with chlorinated silver nanowires on PDMS	Vacuum filtration with mask, spin coating, layer by layer masked self-assembly of CNT	30%	Neutral	CA Non-enzymatic	10.89 µA /mMcm^2	0.05-0.3	[55]
Au/Cr and graphene electrodes on PDMS	Thermal evaporation, photolithography, wet etching, chemical vapour deposition	~30%	Neutral	CA Enzymatic	1 µA/mM	0.01-0.7	[56]
Ag/AgCl ink tattoo	Screen-printing with purchased framed stencils	-	Neutral	CA Enzymatic	23 µA/mM	0.01-0.1	[57]
Au/Ti electrodes with graphene adhered on silk substrate	Electron beam evaporator using nickel mask, chemical vapour deposition, wet etching	-	Neutral	CA Enzymatic	2.5 µA/mM	0.1-10	[58]

1.3.2 Omniphobic surface through hierarchical structures

Hydrophobicity and oleophobicity lead to surfaces with self-cleaning [59,60], anti-icing [61,62] and anti-fouling [63,64] properties. These surfaces are useful for various parts of aircrafts, marine vessels, automobile and medical devices because of such properties. In particular, omniphobic surfaces show repellence towards blood [65], which will be important for point of care devices that requires transfer of such fluid. Point of care is a growing market, expecting to reach US$36.96 billion in 2021 [66]. Hence, there are significant industrial and academic interest in advancing such surfaces (examples of surfaces proposed are tabulated in Table 1.3).

To achieve high hydrophobicity, it had been shown repeatedly that a rough texture is necessary [28,67–71]. As an example, water contact angle increased from 113° for smooth to 172° for hierarchical structures (S/n 19 of Table 1.3). For oleophobicity, hierarchical structures also work better than smooth or single scale texture. In the same study, hexadecane contact angle improved from 67° for smooth to 153° for hierarchical structures. To improve stability of the contact angle, the importance of re-entrant properties (convex structures such as the cavity single-scale structure of Table 1.3) was also introduced [72,73].

Fabrication for such hierarchical or re-entrant structures includes oxygen reactive ion etching, chemical vapour deposition, electrospinning, imprinting and photolithography. The ease and scalability of creating wrinkles through spontaneous buckling makes it a competitive fabrication method for engineering hierarchical structures in the length scale necessary for omniphobicity. Previous paper had reported only on the use of wrinkles (formed from buckling) for hydrophobic surfaces (highlighted in Table 1.3) (highest water contact angle achieved: 172° [23]). The effect of these surfaces to lower surface tension liquid is important. For example, blood has a surface tension of approximately 55 mJ/m^2 [74] and biofouling of oceanographic sensors from oil [75]. There were also few studies (S/n 7, 19 and 20 of Table 1.3) focusing on combination of structures. In addition to fabrication, the use of polymer (e.g. availability of biocompatible polystyrene thermoplastic [76]) as substrates and materials for wrinkles is a more versatile option than some of the structures using metal and fabrics.

In this thesis, the potential of using wrinkles as the foundation for the creation of structures for omniphobicity was studied. It will provide insights into the type of hierarchical structures useful for creating omniphobic surface, which is important for repellence of complex liquid, such as blood.

Table 1.3: Summary of studies on hydrophobicity, oleophobicity or omniphobicity of different surfaces. (θ:contact angle, θ_A: advancing contact angle, θ_R: receding contact angle, α: sliding angle)

S/n	Description of structure	Structure	Liquid	θ	θ_A	θ_R	α	Ref
1	Spin coating of Fluorodecyl polyhedral oligomeric silsesquioxane[77] blend onto surfaces.	Smooth	Water	-	128°	116°	-	[78]
			Hexadecane	-	82°	74°	-	
2	Isophorone diisocyanate and aminopropyl-terminated PDMS polymer brushes on PDMS.	Smooth	Water	-	106°	65°	-	[79]
3	Glass hydrophilized by alkaline treatment, and treated with either decyl-group precursors spin coated on the substrate	Smooth	Water	~96°	102°	93.9°	28.7°	[80]
			Hexadecane	~28°	~30°	~27°	-	
4	Electrospinning polystyrene, fibre-like (µm).	Single scale (fibre)	Water	168°	-	-	2.7 °	[81]
5	PVA crystallized into honeycomb structure. Micro-cavity structures (µm) fabricated.	Single scale (cavity)	Water	133.6°	-	-	<3.6°	[82]
			Hexadecane	94.8°	-	-	-	
6	Graphene adhered to PDMS by etching off from wafer and wrinkled on pre-strained elastomer.	Smooth	Water	105°	-	-	-	[25]
		Single scale (wrinkles)	Water	152°	-	-	-	
7	Silica nanoparticles (nm) on oxygen plasma treated uniaxial rippled PDMS (µm) (pre-strained). Contact angle measured in direction along ripples.	Smooth	Water	112±2°	~112°	~82°	Pinned	[28]
		Single scale (ripples)	Water	124±3°	~140°	~95°	37±6°	
		Single scale (particles)	Water	128±3°	~142°	~80°	58±7°	
		Hierarchical	Water	150±2°	~150°	~138°	16±1°	

S/n	**Description of structure**	**Structure**	**Liquid**	θ	θ_A	θ_R	α	**Ref**
8	Grooves (nm) (imprinted) on wrinkles (µm) (swelled poly(2-hydroxyethyl methacrylate)).	Hierarchical (wrinkles)	Water	~157°	162°	-	<5°	26
9	Nanowrinkles on microwrinkles on polystyrene (oxygen reactive ion etching).	Hierarchical (wrinkles)	Water	166±2°	166±2°	150±2°	12.5°	3
10	Microchannels with wrinkled micropillars on polystyrene (oxygen reactive ion etching).	Hierarchical (wrinkles)	Water	162±2°	-	-	1°	83
11	PA-CVD of carbon coating forming wrinkles (nm) on prepatterned PDMS pillars (µm).	Hierarchical (wrinkles)	Water	160°	-	-	-	24
12	Teflon AF wrinkles on polyolefin (pre-strained)	Hierarchical (wrinkled branches)	Water	172°	175°	172°	<5°	23
13	Electrodeposition of polymer with fluorinated tails for “wrinkled” (more like rough surfaces than wrinkles) surface with spherical structures.	Hierarchical (semi wrinkles)	Water	158°	-	-	3°	84
			Hexadecane	101°	-	-	-	
14	Fractal-like templated silicon oxide layer (nm-µm) on macroporous steel meshes.	Hierarchical	Hexadecane	154±2°	-	-	7±1°	85
15	Coating of clay particles (~1-15 µm) with fluoro solution onto glass slides. Surfaces was rubbed gently.	Hierarchical	Water	155°	-	-	-	86
			Olive oil	151°	-	-	-	
16	Silica TLC plate (8-22 µm) surface coated with Perylene diimide treated silica nanoparticles (40nm).	Hierarchical	Water	156°	-	-	<10°	87

S/n	Description of structure	Structure	Liquid	θ	θ_A	θ_R	α	Ref
17	Multifaceted alumina nanowire forest through electrochemical etching/anodizing.	Hierarchical	Water	170°	-	-	<1°	[88]
			Hexadecane	153.2°	-	-	3°	
18	Fractal-like network of soot created by candle flame coated with silica shell (nm to µm)	Hierarchical	Water	165 ± 1°	-	-	1 ± 1°	[89]
			Hexadecane	156 ± 1°	-	-	5 ± 1°	
19	Ultrathin metal films deposited on glass surface and etched into nano-pillars (nm). Secondary structures (nm- µm) deposited by nanospray combustion chemical vapour deposition process.	Smooth	Water	113 ± 3°	-	-	-	[90]
			Hexadecane	67 ± 2°	-	-	-	
		Single scale (nanopillars)	Water	144 ± 4°	-	-	-	
			Hexadecane	104 ± 3°	-	-	-	
		Hierarchical (branching)	Water	165 ± 3°	-	-	<3°	
			Hexadecane	150 ± 3°	-	-	<6°	
		Hierarchical (pillars & branching)	Water	172 ± 4°	-	-	<3°	
			Hexadecane	153 ± 3°	-	-	<6°	
20	Electrospun surfaces from fluorodecyl POSS molecules blended with PMMA to create beads (µm), beads-on-strings (nm- µm) and fibre (µm) structure. Micro-hoodoo (cavity like) re-entrant surfaces (3-20 µm) from photolithography.	Single scale (beads)	Water	-	>160°	>160°	-	[72]
			Hexadecane	-	156°	150°	~5°	
		Single scale (fibre)	Water	-	>160°	>160°	-	
			Hexadecane	-	153°	134°	-	
		Single scale (cavity)	Water	-	>160°	~160°	-	
			Octane	-	162°	144°	-	
		Hierarchical (beads on strings)	Water	-	>160°	>160°	-	
			Hexadecane	-	153°	141°	-	

S/n	**Description of structure**	**Structure**	**Liquid**	θ	θ_A	θ_R	α	**Ref**
21	PDDA layer, silica nanoparticles layer and other chemical sprayed onto glass (using spray gun). Optical micrographs are unclear on structures, AFM seems to suggest hierarchical.	-	Water	163 ± 1°	-	-	2 ± 1°	[91]
			Hexadecane	157 ± 1°	-	-	4 ± 1°	
22	Silica nanoparticles mixed in methylphenyl silicone resin and dip coated onto poly(ethylene terephthalate) substrate. AFM unclear on structure.	-	Water	170 ± 2°	-	-	1 ± 1°	[92]
			Hexadecane	153 ± 2°	-	-	4 ± 1°	
23	Small with thick and long silicone nanofilaments stacked into 4 µm thick layer on glass. No SEM for the specific conditions listed for the contact angles.	- (strings)	Water	173.1°	-	-	1.3°	[93]
			Hexadecane	174.4°	-	-	2°	

1.4 Background

1.4.1 Various methods for creating wrinkles

One of the earliest techniques used for fabrication of wrinkles is the deposition of metal films onto thermally expanded PDMS [1]. The deposition of a stiff film onto a substrate and subsequent compression of the substrate causes the stiff film to buckle into wrinkles to relieve the compressive stress. There are generally two strategies used for creating such stiff films on a substrate, deposition of a secondary layer on the substrate or modification of the surface of the substrate.

There are various methods to deposit secondary layers onto substrates, ranging from the conventional sputtering or transfer of metal/film onto pre-strained PDMS [1,17], spin-coating of conducting polymer or Teflon onto thermo-retractable/pre-strained polystyrene sheet [23,37], to electroless deposition of gold onto pre-strained polystyrene [94]. Examples of modification of the surfaces of substrate are the use of oxygen reactive etching of pre-strained polystyrene [3], oxygen plasma treatment of pre-strained PDMS [31], UVO treatment of pre-strained PDMS [4,5,95], argon ion beam treatment on PDMS [96] or UVO treatment of polystyrene with swelling induced compression [97].

In this thesis, a technique from each strategy was used, electroless deposition of gold onto pre-strained polystyrene [94] and UVO treatment of pre-strained polystyrene. UVO treatment was reported to increase the cross-linking between polymer chains, increasing the elastic modulus with longer treatment time [98]. Surprisingly, to the best of the author's knowledge, UVO treatment has yet been reported to be used on pre-strained polystyrene in literature for the fabrication of wrinkled substrate. Both methods do not require expensive specialised equipment and can be done rapidly.

Pre-strained polystyrene has the advantage of being widely and cheaply available. It also provides a high strain in two dimensions through a simple thermal treatment. The polystyrene used in this thesis will shrink approximately 60% in two dimensions when heated to approximately 140°C for a few minutes.

In the following section, a common model for describing the buckling of film relevant to this work will be introduced, showing the importance of having increased elastic modulus (through metal film or UVO treatment) and constant strain.

1.4.2 Buckling of film into wrinkles

The wrinkling studied in this thesis uses compressive wrinkling as oppose to tension-induced wrinkling. Such systems involve thin films bonded to substrates. The stiffness differential between the film and substrate leads to buckling of the surface into wrinkles after compression (Figure 1.1). A commonly used model for low strain uniaxial buckling of a film in sinusoidal pattern provides several well-known equations. These equations are solution to a system with compressive force on the elastic film on an elastic substrate with shear stresses between the film and substrate neglected [99]. The system can be described by a differential equation, the classical equation for bending of a stiff film on complaint substrate, with sinusoidal deflection as valid solution [99,100].

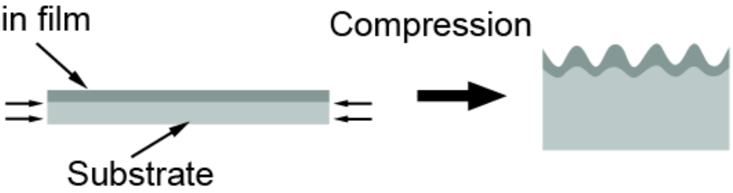

Figure 1.1: Illustration of the buckling process.

Solving for the wavelength that minimized force with respect to wavelength, the expected wavelength is [99,100]

$$\lambda = 2\pi d\left(\frac{\bar{E}_{film}}{3\bar{E}_{substrate}}\right)^{1/3} \tag{1}$$

where $\bar{E} = E/\left(1-v^2\right)$ is the plain-strain modulus and v is the Poisson's ratio.

Using the critical stress (applied force at critical point divided by cross-sectional area of film) [100], the critical strain required for the film to buckle is [99],

$$\varepsilon_c = \frac{1}{4}\left(\frac{3\bar{E}_{substrate}}{\bar{E}_{film}}\right)^{2/3} . \tag{2}$$

Using the difference between applied strain and critical strain, the amplitude of the buckles is approximated by [100],

$$A = d\left(\frac{\varepsilon}{\varepsilon_c}-1\right)^{1/2} . \tag{3}$$

Another analytical method is based on minimizing the total energy of the film and substrate [101] and provides the same results. These equations assisted in understanding wrinkles in many literature [4,102–104]. However, these equations are shown to be valid only to strain of up to approximately 5% [105].

The random buckling of a substrate experiencing much higher strain is more complex. For UVO treated pre-strained PDMS, it was suggested that the amplitude will saturate at a certain strain and this will cause the wrinkled surface to act as a thicker and stiffer film for subsequent repeated buckling [15]. From the scanning electron microscope (SEM) image of 3 min UVO treated and shrunken polystyrene, the subsequent buckling may be referring to the boundaries of the wrinkles as indicated by the arrows (Figure 1.2). In our samples, there are clearly more than one or two generations of wrinkles.

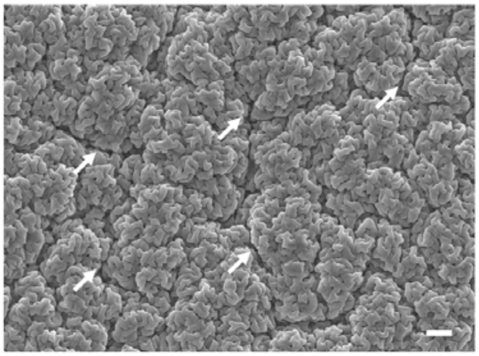

Figure 1.2: SEM of shrunken 3 min UVO treated pre-strain polystyrene. White arrows indicate the boundaries showing folds. Scale bar is 1 μm.

To study large strain, another set of equations are suggested based on geometrical nonlinearity and nonlinear constitutive model [106]. This results in a model with wavelength given as [106],

$$\lambda = \frac{\lambda_0}{(1+\varepsilon)(1+\xi)^{1/3}} \tag{4}$$

where λ_0 is the wavelength given by the previous set of equations and $\xi = 5\varepsilon(1+\varepsilon)/32$ and

$$A = \frac{A_0}{\sqrt{1+\varepsilon_{pre}}\,(1+\xi)^{1/3}} \tag{5}$$

where A_0 is similarly given by the previous set of equations. These set of equations suggest that wavelength and amplitude decreases as strain increases which is consistent with experimental results of buckled silicon structures on pre-strain PDMS [106]. This is different from the first set of equations which predicted that wavelength only depends on modulus and Poisson's ratio.

From these theoretical equations, it is clear that by introducing a layer of controlled stiffness on the surface of pre-strain polystyrene and a consistent strain via thermal shrinking, buckling can be induced, and wrinkles of consistent dimensions can be formed on the polystyrene substrates. After fabrication of the wrinkles, the devices were tested for their performance through different characterisation techniques. The techniques are described in the following sections.

1.4.3 Electrochemical sensing

Electrochemical sensing is the detection of the flow of electrons during reduction and oxidation in a solution. The presence of certain analyte in the solution will result in oxidation or reduction given the right conditions, changing the current which can be measured. This provides a method to determine the concentration of said analyte.

The usual set-up for electrochemical sensing is an electrochemical cell, which includes a working electrode, reference electrode, counter electrode, electrolyte solution and potientostat. The working electrode is where the analyte chemical reaction of interest happens. A potentiostat is fixed to the working electrode, providing it with selected applied potential difference to the reference electrode. As the reaction of interest happens at the working electrode, it is important for it to be clean. Hence, it is usually polished before use to remove unwanted species [107]. This can be done electrochemically through sulphuric acid cyclic voltammetry (CV) scans [108]. As some analyte adsorb on the surface during measurements, causing interference, cleaning steps can be required between measurements [107].

The reference electrode provides a stable and known potential which applied potential for the other electrodes can be based upon [107]. In this work, a common reference electrode, the Ag/AgCl electrode, was used. Pseudo reference electrodes are sometimes used when macro electrodes are not suitable. These electrodes can be simple metal wires and one major difference with usual reference electrodes is that they do not have a potential that is independent of the electrolyte [109].

The counter electrode serves to complete the circuit through the solvent, allowing current to flow from working electrode. The size of the counter electrode is usually bigger than the working electrode, to ensure that its kinetics of reaction will not affect those at working electrode [107].

The solvent used should dissolve the analyte and the electrolyte, and be stable in the potential range under study [107]. The analyte will receive or transfer electrons at the electrodes while the electrolyte, used to decrease the resistance of solution, balances the charges being moved.

After setting up an electrochemical cell, one important characteristic of the working electrode is the electroactive surface area, also known as the real surface area. As the surface of the electrode is not always smooth, the actual electrochemically active area can surpass the geometric area [110]. As electrochemical activities occur on surface active areas, it is important to monitor the electroactive surface area during changing conditions in experiments.

For a gold working electrode, the electroactive surface area can be determined by sulphuric acid CV scans. A positive sweep of potential will result in formation of gold oxide layer, with anodic peaks relating to various oxidation reactions [111] (at ~1-1.4V with reference to Ag/AgCl [53]):

$$\begin{aligned} &Au + H_2O \rightarrow AuOH + H^+ + e^- \\ &AuOH \rightarrow AuO + H^+ + e^- \end{aligned} \tag{6}$$

The return sweep results in a cathodic peak due to the reduction of the oxide layer (at ~1-0.8V with reference to Ag/AgCl [53]). The charge involved in this process was approximated to be 0.386 mC/cm^2 [112]. By integrating the cathodic peak, considering the baseline, the electroactive surface area can be estimated using the approximated charge.

Finally, the sensitivity of the electrodes for detection of glucose concentration can be examined. For non-enzymatic glucose sensors, signal is generated by directly oxidizing glucose on the surfaces of the electrodes. It was believed that the metal will form a metal oxide layer, which forms surface bound OH radicals, which can oxidize reactants near the surface, such as glucose [113]. As the reduction potential of oxygen is more positive than glucose oxidation, a potential can be chosen to minimize this issue [113]. With the right potential, which can be determined via cyclic voltammetry through observation of the appropriate glucose oxidation peak, amperometric measurement can be used to record signals for different glucose concentration. By fitting a linear line through the current measured for different concentration, the sensitivity (slope) can be determined.

1.4.4 Sheet resistance

Resistivity ρ (Ωcm), is described as the ratio of electric field, E (Vcm^{-1}) to current density, J (Acm^{-2}) [114]. In this work, the resistivity of the strained wrinkled electrodes is an important performance indicator as it provides a way to predict the current density that could be detected with an input electric field, which is relevant to electrochemical sensing. While resistivity is the property of interest, resistance is the quantity to be determined first.

The standard way to determine resistance is by measuring the voltage drop between two points by running a known current though the electrodes. This is usually inaccurate as it includes the voltage drop due to contact resistances at the probes. Even though the reported contact resistances of gold, the material used in this work is low, in the range of milliohms [115], for accuracy, the measurements in this work were done via 4-point probe technique (Figure 1.3). This technique makes use of the assumption that if the current is injected through separate probes from the voltage probes, there will be no voltage drop through the voltage probes. This assumption will hold if the impedance of the voltage probe can be considered to be infinite.

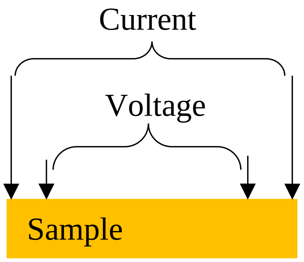

Figure 1.3: Illustration of a 4 point probe set-up.

Now that the resistance can be measured accurately, the resistivity or sheet resistance of the material can be determined. For a thin film, sheet resistance, is proportionate to resistivity, and is a more common performance indicator than resistivity. As the thickness of the gold film used in this work was approximately 50nm [94], sheet resistance will be used. When the ratio of the thickness of the gold film (~nm) to the spacing between the probes (~mm) is much less than one, the gold film can be assumed to be an 2D sheet [114]. With probes placed on the edge of the sample, it can be considered to be the case of a semi-infinite 2D sheet and a well-known correction factor can be used to determine the sheet resistance from the measured resistance [114],

$$\frac{\pi}{\ln 2}\frac{V}{I} \ . \tag{7}$$

The sheet resistance measurements will assist in determining if the electrochemical sensing results are reasonable and reliable. Other than electrochemical sensing and resistance measurements, the other important characterisation done is this work was for omniphobicity.

1.4.5 Omniphobic characterisation

Omniphobicity is the study of the wettability of surfaces, specifically examination of the ability of surfaces to repel both low and high surface tension liquid. Characterisation of such surfaces starts from examining the behaviour of a sessile droplet placed on the surface. Such experiments are done generally through commercial goniometer, which provides a liquid dispensing unit, movable sample table, backlight for the droplet and a charge-coupled device camera with a software that does curve-fitting on the profile of the droplet.

On an ideal smooth surface, the droplet, as shown in Figure 1.4, will result in a static contact angle (θ) which depends on three interfacial surface tensions, solid liquid (γ_{SV}), solid vapour (γ_{SV}) and liquid solid (γ_{LS}). The relationship between these three surface tensions and the static contact angle is given by a well-known equation (Young's relation) [116],

$$\gamma_{SV} = \gamma_{LV} \cos\theta + \gamma_{SL} \tag{8}$$

This relation indicates that low surface tension liquid will have lower contact angle, θ, due to smaller θ_{LV}.

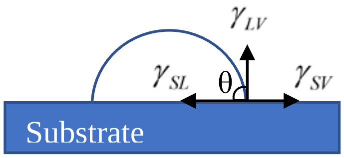

Figure 1.4: Illustration of vectors in a sessile droplet in relation to the Young's relation. Adapted /from paper [117].

There are several common performance categories for such surfaces [118]. Depending on the water contact angles, a surface is hydrophilic ($\theta < 90°$) or hydrophobic ($\theta > 90°$). Depending on contact angles of low surface tension liquids (oil, alcohol or organic solvent), a surface is oleophilic ($\theta < 90°$) or oleophobic ($\theta > 90°$). Surfaces that are both hydrophobic and oleophobic are consider omniphobic. In extreme cases, surfaces can be categorized as super-repellent. With high water contact angles ($\theta > 150°$) and low contact angle hysteresis (usually $< 5°$) [119], the surfaces are considered to be superhydrophobic. Similarly, for low surface tension liquids, if there are high contact angles and low contact angle hysteresis, the surfaces can be referred to as superoleophobic [119]. Surfaces that are both superoleophobic and superhydrophobic are referred to as superomniphobic [119] or superamphiphobic [120].

To achieve such repellent surfaces, the usual strategy is by having textured surfaces. For non-textured surface, the maximum reported contact angle is approximately 130° [119], which was achieved through having a low surface free energy coating [121]. To go beyond such limitations, studies [28,67–71] have shown the viability of textured surfaces. The two popular and widely used models describing the behaviour of sessile droplets on such textured surfaces are the Wenzel model [68] and Cassie model [69]. Wenzel model describes scenario where the droplet fully wetted the surface of the textured surface while Cassie model describes scenario where there is non-wetted area of contact between the droplet and textured surface (Figure 1.5).

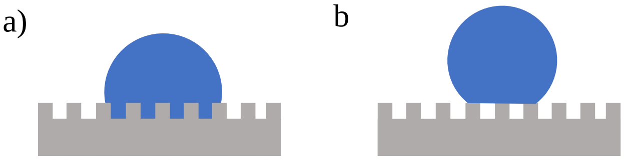

Figure 1.5: Illustration of a droplet on textured surfaces. a) Wetted contact between a droplet and a textured surface in the Wenzel regime. b) Non-wetted contact between a droplet and a textured surface in the Cassie regime.

The Wenzel relation for estimating the static contact angle, θ_w, for the wetted stated is [68],

$$\cos\theta_w = r\cos\theta \quad , \tag{9}$$

where r is the ratio of the actual surface area in contact with the droplet to the projected surface area of the droplet. The equation indicates that with $r > 1$ for a rough surface, when $\theta > 90^\circ$, θ_w will be higher but when $\theta < 90^\circ$, θ_w will be lower. Hence, the Wenzel regime accentuates hydrophobicity and hydrophilicity. This means that for low surface tension liquid with $\theta < 90°$, a high contact angle is still not possible.

However, not every scenario will have the droplets fully wetting the textured surfaces. For the Cassie regime, the contact angle for a droplet, θ_C, can be estimated as [69,119,122],

$$\cos\theta_C = f_{SL}\cos\theta + f_{LV}\cos\pi = f_{SL}\cos\theta - f_{LV} \tag{10}$$

where f_{SL} is the ratio of the total area of solid-liquid interface to the projected area of the drop and f_{LV} is the ratio of the liquid-air interface to the projected area of the drop. Due to the addition of the term f_{LV}, it is possible for even low surface tension liquid with low Young's relation contact angle, $\theta < 90°$, to achieve a high contact angle, $\theta_C > 90°$.

In addition to having single length scale textured surfaces, contact angle can also be approximated for hierarchical structures by rewriting Cassie relation recursively [123],

$$\cos\theta_{c,n} = \left(1 - f_{LV,n}\right)\cos\theta_{c,n-1} - f_{LV,n} \tag{11}$$

where $n = 1, 2, 3, \ldots$ corresponding to the number of length scale of texture, with larger n corresponding to larger length scale. This equation indicates that increasing the number of length scale will increase the contact angle, $\cos\theta_{c,n}$ [119].

For droplets in the Cassie regime, when considering liquid of different surface tension, it is also important to look at the local geometric texture. This is because the liquid is expected to form a contact line at the local structure equal to the angle based on Young's relation [119]. For a stable Cassie regime, the Young's relation angle (θ) must be higher than the local contact angle (ψ) [119]. Hence, it is to be noted that a convex structure, also known as the re-entrant texture [119], is much better for low surface tension liquid (Figure 1.6).

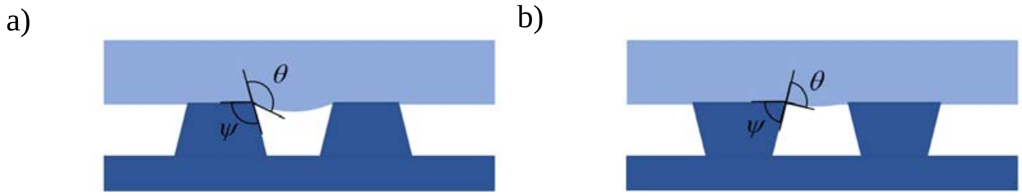

Figure 1.6: Illustration of interaction between a droplet and local texture. a) A concave structure ($\psi > 90°$) with a high surface tension liquid ($\theta > 90°$). b) A convex structure ($\psi < 90°$) with a low surface tension liquid ($\theta < 90°$). Adapted from paper [119].

Other than contact angle, as mentioned earlier, contact angle hysteresis ($\theta_A - \theta_R$ as shown in Figure 1.7) is part of characterisation of superhydrophobicity or superoleophobicity. However, for self-cleaning surfaces, the property of interest is the adhesion of the droplet on the surfaces, which relates to sliding or rolling-off angle. Hence, in this work, the sliding angle will be measured instead of contact angle hysteresis. Regardless, it is useful to note that contact angle hysteresis was shown to be well correlated to rolling-off or sliding angle for droplets in Cassie regime [124] and is an indicator of the changes in liquid solid interfacial tension due to the different condition when droplet is advancing compared to when receding [124].

Sliding angle, α, is the tilt angle when the droplet starts sliding and directly shows the adhesiveness of the surface. A higher sliding angle means higher adhesiveness. The sliding angle is dependent on the gravity ($mg\sin\alpha$) and the friction (f) due to the adhesiveness of the surface (Figure 1.7).

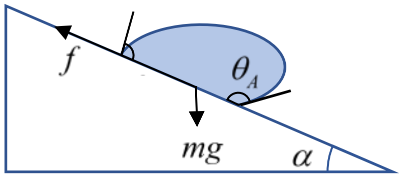

Figure 1.7: Illustration of droplet on a tiled surface with an angle α .

1.5 Thesis overview

Chapter 2 reports a process to create stretchable electrodes by transferring wrinkled gold electrodes onto elastic substrates. The electrochemical sensing area of the electrodes were quantified and compared to electrodes pre-transfer. The electrodes are tested with glucose to show the applicability for electrochemical sensing with and without strain. The resistivity of the electrodes was studied under strain to provide understanding of the electrochemical sensing behaviour.

Chapter 3 reports a process that can be used to create surfaces with different types of structures: nano-structures, micro-structures or both. The wrinkles are decorated with nanoparticles to achieve hierarchical structures. The different surfaces are tested for water, oil and blood repellence

The final chapter summarises the conclusions in chapter 2 and 3, elaborates on the contributions of this thesis and introduces some future work that can be done.

Chapter 2

Stretchable electrodes

2.1 Chapter introduction

This chapter detailed the fabrication of stretchable wrinkled gold electrodes. The electrodes were used for electrochemical sensing under strain and tested for specifically for detection of glucose concentration. The various objectives for the thesis are addressed here.

Objective 1: Here, a process that takes less than three days to create stretchable electrodes are introduced. More than ten samples can also be done using the process in one batch. Specifically, the process includes electroless deposition of gold on polystyrene, thermal treatment to induce wrinkles, curing of elastomer (Ecoflex) onto the samples and the dissolution of polystyrene. It is entirely solution based, requiring only the use of bench-top craft cutter, air plasma cleaner, heat plate and oven. The process allows us to fabricate good quality wrinkled electrodes on elastomer in a few days. Such easy and fast procedures are valuable for rapid prototyping of devices.

Objective 2: The stretchable electrode's viability towards electrochemical sensing under strain was considered. To increase the robustness of the stretchable electrode, aminosilane was used to provide improved adhesion between the Ecoflex and the wrinkled gold surface. Based on the CV scans of the electrodes and polystyrene and Ecoflex, the transfer process had not affected the electroactive surface area significantly. The sensitivity of the stretchable electrode to glucose was determined, using pulsed amperometric detection using conventional Ag/AgCl reference electrode. The current measured had good linearity of from 0.1 to 10 mM glucose concentration. The sensitivity was 860 µA/mM.cm^2, which is approximately 8% larger than wrinkled and nanoporous gold electrodes previously reported [53]. It was also shown that electroactive surface area remained consistent up to a 45% strain. These show that the electrodes fabricated is feasible for stretchable electrochemical sensing.

Objective 3: In this work, it was also shown that the stretchable electrodes are viable as a glucose sensing device. An on-chip electrochemical cell was fabricated, using a pseudo-reference electrode, which brings it closer to an applicable device. The sensitivity towards glucose was measured to be 730 ± 80 µA/mM.cm^2, which is a comparable value to external reference electrode. For strain, the current was measured for 5 mM of glucose. It slightly increased up to 25% strain and stayed consistent up to 45%. The resistance measurements are consistent was the electrochemical measurements. It showed that when the strain is perpendicular to the current, similar with the electrochemical set-up, the resistance decreases gradually when strain increases, concurring with the increase in current measurements for 5 mM of glucose. In addition, when the strain is parallel to the current, the resistance is constant up to 30%. Both the electrochemical sensing and resistance measurement demonstrated the potential of the fabricated electrodes for use as skin-tight electrochemical glucose sensing device.

As reproduced from the preface, this paper consisted of contributions by Marta Skreta and Hannah McPhee, Sudip Saha and Ryan Deus who, with inputs from the author, assisted with: (a) refinement of the electrode transfer process initiated by the author, (b) collection of electrochemistry and resistivity data, and (c) providing written preliminary analysis of electrochemistry and resistivity data. Strain set up and surface characterisation was done by the author. Overall analysis and presentation of data was adjusted and revised by the author. Manuscript was written mainly by the author. Dr. Soleymani assisted with helpful suggestions and revision of the manuscript.

Paper is submitted to Analyst (published by Royal Society of Chemistry) on 22 Aug 2018, under revision

Solution-Processed Wrinkled Electrodes Enable the Development of Stretchable Electrochemical Biosensors

Yuting Chan [a], Marta Skreta [a], Hannah McPhee [a], Sudip Saha [b], Ryan Deus [a], Leyla Soleymani [a,b,*]
[a] McMaster University, Department of Engineering Physics, 1280 Main Street West, Hamilton, L8S 4L7, Canada
b McMaster University, School of Biomedical Engineering, 1280 Main Street West, Hamilton, L8S 4L7, Canada
* Corresponding author. E-mail address: soleyml@mcmaster.ca (L. Soleymani)

2.2 Abstract

Wearable biosensors are critical for enabling real-time and continuous health monitoring and disease management. Conductors that retain their conductivity under strain are an essential building block of these systems. Strategies based on stretchable materials or structures have enabled the development of electrodes that can withstand impressive strains before loss of conductivity. In spite of this, it remains challenging to develop three-dimensional and high surface area electrodes that combine stretchability with high analytical sensitivity. Here, we develop stretchable electrochemical biosensors using solution-processed wrinkled gold electrodes. Wrinkling enhances the surface area of the electrodes and allows glucose to be detected with a sensitivity of 860 µA/M.cm2. Furthermore, wrinkling enables electrodes to be strained by up to 100% without significant loss in conductivity.

2.3 Introduction

Wearable biosensors are envisioned to improve human health by enabling continuous disease management and real-time health monitoring [1,2]. Stretchable conductors are a key building block in constructing the transducing elements [3–5] or the interconnects [6–8] of biosensing systems. Specially-designed *materials* or *structures* [9,10] are used to create electrodes that preserve their conductivity upon stretching. Stretchable materials are created by combining conductive elastomers with networks of conducting building blocks such as silver nanoparticles [11] or nanowires [12], graphene [13], or carbon nanotubes [14]. These materials have moderate conductivity under strain as the contact between their conductive building blocks diminishes [9]. Stretchable structures are created based on geometries such as wrinkles [15], coils [16], sponges [17], and meshes [18], which allow the conductor to unfold or deform under strain. These structures enable high conductivity materials to be incorporated in a stretchable framework and maintain conductivity by minimizing breaks.

Wrinkled films are created when a compliant substrate modified with a stiff skin experiences compressive stress or the removal of tensile stress. The wrinkled geometry allows the applied strain to be relieved through unfolding and alignment of the wrinkles. As a result, stretchable electrodes, withstanding strains of up to 400% are created using conductive wrinkles [7,19,20]. Additionally, the micro/nanoscale features of the wrinkled films significantly increase the electrochemical signal [21] and analytical sensitivity [22,23] of chemical and biological sensors.

The combination of enhanced analytical performance and stretchability makes wrinkled electrodes ideally suited for use in wearable sensors. Our goal was to develop stretchable biosensing electrodes with a wrinkled architecture using a facile, *yet scalable*, fabrication method. Solution-processed electrodes, where the precursors or building blocks of the conductive film are dispersed in a solvent removed during processing, offer great promise for this purpose. Solution-processing eliminates the need for vacuum-based equipment operated in cleanrooms and it is also applicable to large-area and high-volume manufacturing using roll-to-roll processes [24].

2.4 Results and discussion

2.4.1 Fabrication of stretchable wrinkled electrodes using solution-processing

To create wrinkled electrodes on stretchable substrates, we fabricated solution-processed wrinkled electrodes [23,25] on the surface of pre-strained polystyrene and transferred them to stretchable elastomers [7,20]. Pre-strained polystyrene shrinks when it is heated above its glass transition temperature [26]. When the surface of pre-strained polystyrene is modified with a stiff skin, the compressive stress imposed on the skin layer causes it to crumple, leading to the creation of wrinkled films [27]. To create wrinkled electrodes on stretchable substrates, we used the process schematically demonstrated in Figure 2.1(a). We defined the electrode pattern using a vinyl mask adhered onto a pre-strained polystyrene substrate modified with an aminosilane linker. We then deposited a gold nanoparticle seed layer on the polystyrene surface by leveraging on its electrostatic interactions with the linker layer. We created a continuous gold film on the seed layer using electroless deposition. Following heat shrinking, a wrinkled gold film was created on the shrunk polystyrene substrate (Figure 2.1(b)); however, this substrate was rigid and not applicable to stretchable biosensors. To transfer the electrodes to a stretchable substrate, we poured Ecoflex, a silicone elastomer, onto the wrinkled electrodes, and dissolved the polystyrene substrate after the Ecoflex had cured [7]. This transferred the wrinkled electrodes from rigid polystyrene to stretchable Ecoflex.

We compared the sheet resistance of the electroless deposited gold on polystyrene to the transferred gold on Ecoflex (Figure 2.1(b)). The sheet resistance of gold on polystyrene is 0.33 ± 0.03 Ω/□, and is comparable to a previously reported value [28], whereas the transferred wrinkled gold has a higher value. This higher resistance in the transferred film is expected since the transfer process introduces breaks into the previously continuous film due to the swelling of the Ecoflex during solvent processes [7,20]. The value obtained here is lower than the previously reported resistance for stretchable wrinkled gold electrodes (85 ± 3 Ω/□). [7]

To understand the structural differences between the wrinkled films created on polystyrene and those transferred to Ecoflex, we performed top-view and cross-sectional imaging using electron microscopy. The top-view scanning electron microscope (SEM) images showed that wrinkles on the surface of Ecoflex are significantly smaller in wavelength than those on polystyrene (Figure 2.1(c)). To further examine this structural difference, we performed cross-sectional transmission electron microscopy (TEM) on the wrinkles positioned on Ecoflex and polystyrene (Figure 2.1(c)-inset). We observe that the wrinkled gold film is rooted in the polystyrene substrate, interfaced with polystyrene on the bottom side and with air on the top side. When the wrinkled film is transferred from polystyrene to Ecoflex, the side of the wrinkles interfaced with polystyrene becomes the top-most surface. We hypothesize that when the gold film is compressed on the polystyrene substrate, it is easier for the crests, surrounded by air, to overlap one another forming *folds* while the troughs, embedded in polystyrene, rarely overlap. As a result, the surface of the wrinkled film on polystyrene is dominated by large folds, whereas, the surface of the wrinkled film on Ecoflex is dominated by small troughs, leading to the significant structural difference observed in these two materials architectures.

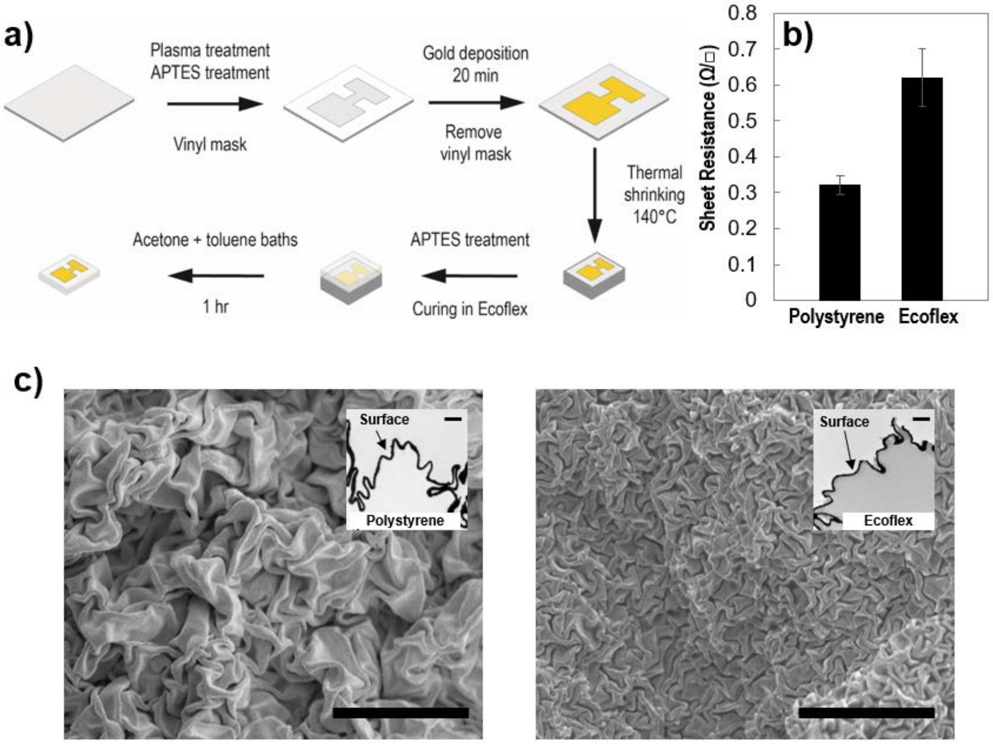

Figure 2.1. Fabrication of solution-processed electrodes on stretchable substrates. (a) Schematic of fabrication process for wrinkled electrodes on Ecoflex. (b) Sheet resistances of wrinkled gold film on polystyrene and Ecoflex. (c) Scanning electron microscope images of wrinkled film before (left) and after (right) transfer from polystyrene to Ecoflex (scale bars are 10 µm). Insets show the transmission electron microscope images of the cross-section of the wrinkled film (scale bars are 1 µm).

2.4.2 Enzyme-free glucose sensing and electrode sensitivity

Following the successful fabrication of solution-processed wrinkled gold electrodes on stretchable substrates, we investigated the suitability of these electrodes for electrochemical sensing. We analyzed their electrochemical surface area using cyclic voltammetry (CV) and their ability to oxidize glucose using chronoamperometry. Lastly, we compared their performance with the wrinkled gold electrodes fabricated on polystyrene (Figure 2.2). The CV of the gold electrodes recorded in an acidic solution demonstrated the expected redox signature for gold (Figure 2.2(a)). For wrinkled electrodes before *and* after transfer to the stretchable substrate, oxidation of gold occurred between +1.0 and +1.5 V in the forward scan. In the reverse scan, the characteristic reduction peak of gold oxide occurred at approximately +0.8 V. Additionally, transferring the wrinkled gold layer from polystyrene to Ecoflex did not significantly vary the electroactive surface area (≤ 5 % variation). These results indicate that the transfer process allows the electrical and electrochemical properties of gold to be preserved.

We investigated whether it would be possible to use the wrinkled electrodes created here for developing biosensors. We used pulsed amperometric detection (PAD) to monitor the concentration of glucose in the clinically-relevant range of 1-10 mM [29,30]. PAD is ideally-suited for use in wearable biosensing systems because it offers built-in surface cleaning [31,32] and extends the linear range of the biosensors [23]. This method uses a multistep potential waveform (Figure 2.2(b), (c)) for anodic cleaning (+0.80 V), cathodic regeneration (-0.60 V), and detection of glucose (0.27 V) [23,31,33]. The current obtained following the detection pulse was averaged and plotted as a function of glucose concentration (Figure 2.2(d)). We compared the performance of the polystyrene and Ecoflex electrodes for enzyme-free oxidation of glucose by comparing their sensitivities. To calculate the sensitivity, the slope of each curve was taken and adjusted for the geometric surface area. It was found that the polystyrene and Ecoflex electrodes had sensitivities of 710 and 860 µA/mM.cm^2 respectively (Figure 2.2(e)). The enhanced sensitivity of the Ecoflex electrode is related to the reduction in the geometric surface area following the transfer process (Figure 2.2(e)). The solvent steps used for dissolving polystyrene swell and shrink the Ecoflex layer [7,20], which decrease the two-dimensional footprint of the gold electrode. The sensitivity of the Ecoflex electrodes is slightly (~8%) larger than the wrinkled and nanoporous gold electrodes previously reported for enzyme-free glucose biosensors made from gold [23]. This demonstrates that fabricating wrinkled gold electrodes by solution-processing and materials transfer leads to stretchable biosensors with excellent analytical performance.

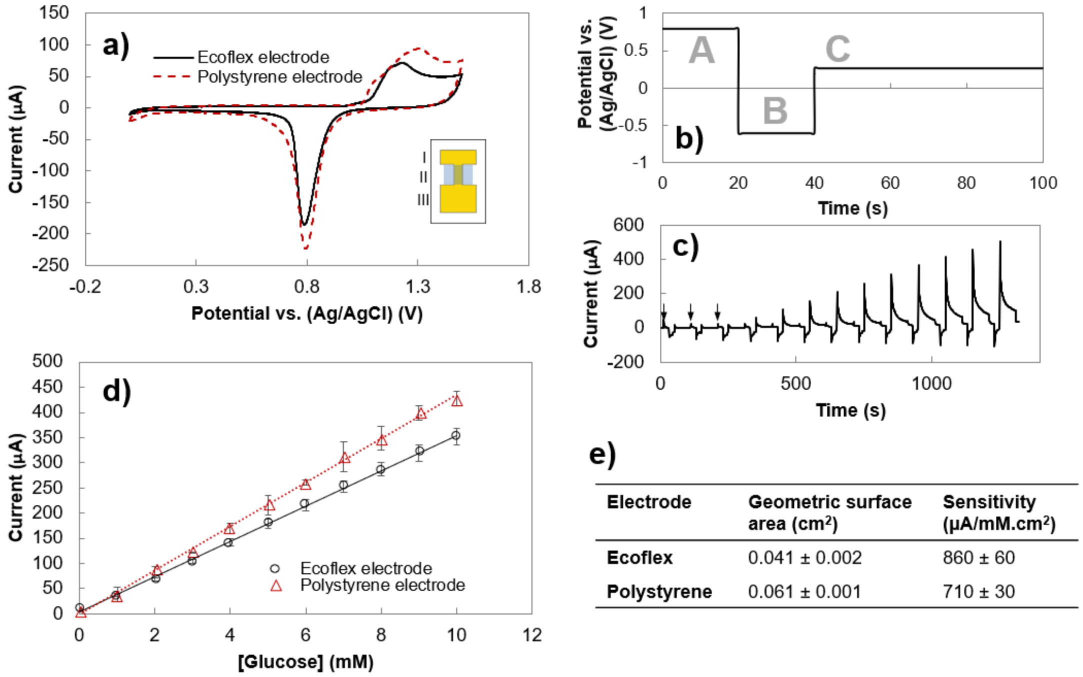

Electrode	Geometric surface area (cm^2)	Sensitivity (µA/mM.cm^2)
Ecoflex	0.041 ± 0.002	860 ± 60
Polystyrene	0.061 ± 0.001	710 ± 30

Figure 2.2. Electrochemistry using solution-processed wrinkled electrodes on stretchable substrates. (a) Cyclic voltammogram of polystyrene (dash) and Ecoflex electrodes (solid) in 0.05 M H_2SO_4 at a scan rate of 0.05 V/s versus a Ag/AgCl reference electrode. The electrode is illustrated in inset: (I) contact pad, (II) insulated gold wire, and (III) working electrode surface. (b) A multi-step potential waveform was applied to the working electrode for detecting glucose. The portion marked A indicates the first step of the waveform (anodic cleaning), the portion marked B indicates the second step of the waveform (cathodic regeneration), and the portion C indicates the third step (analyte detection). (c) Pulsed amperometric signal of the wrinkled gold electrode. During the first three pulses (indicated by arrows), 1 mM KCl was added to ensure signal stability. Each signal thereafter was generated by adding 1 mM glucose. (d) Calibration curve plotting current as a function of glucose concentration for polystyrene (triangle) and Ecoflex (circle) electrodes. The current was extracted from the first 5 seconds of the C pulse in the pulsed amperometric signal. All error bars represent one standard deviation. (e) Table summarizing the analytical sensitivity and geometric surface area for each class of electrode.

2.4.3 Electrochemistry under strain

To assess the performance of the stretchable electrodes, we sought to measure their electrochemical current under strain. For this purpose, we created an on-chip electrochemical cell, where the working, counter, and reference electrodes were integrated on a single substrate [28]. Using this setup, the electrochemical response of the electrodes was measured, directly in the electrolyte, while different amounts of strain were applied to the substrate (Figure 2.3(a)). The performance of on-chip electrochemical cell was evaluated by performing CV in 0.05 M sulfuric acid (Figure 2.3(b)). The CV showed the expected redox signature of gold in acidic solutions with a broad peak related to the oxidation of gold and a sharp peak indicating the reduction of gold oxide. However, the peak potentials were shifted compared to the response observed when a conventional off-chip reference electrode was used (Figure 2.2(a)). This is expected as the electrochemical potential for the gold pseudo-reference electrode is different from the potential of the conventional Ag/AgCl electrode [34]. We also evaluated the on-chip electrochemical cell in detecting glucose using the PAD method used with the single electrode chips (Figure 2.3(c)). The sensitivity of the on-chip electrochemical cell in response to glucose is 730 ± 80 μA/mM.cm^2, which is comparable to the values obtained with polystyrene and Ecoflex electrodes. This indicates that using on-chip reference and counter electrodes does not significantly affect the observed electrochemical behaviour.

To evaluate the ability of the glucose sensor to operate under strain, we measured the electroactive surface area of the working electrode under different strain values (Figure 2.3(d)). The electroactive surface area did not change significantly as strain was increased or decreased. We then tested the ability of the on-chip electrochemical cells to detect 5 mM of glucose under strain (Figure 2.3(e)). As the strain was increased, the electrochemical current showed an increasing trend up to a strain of 25%, after which the current remained constant. This increasing trend was different from the behaviour observed in previous studies, where applying strain decreases or does not change the measured current [7,19].

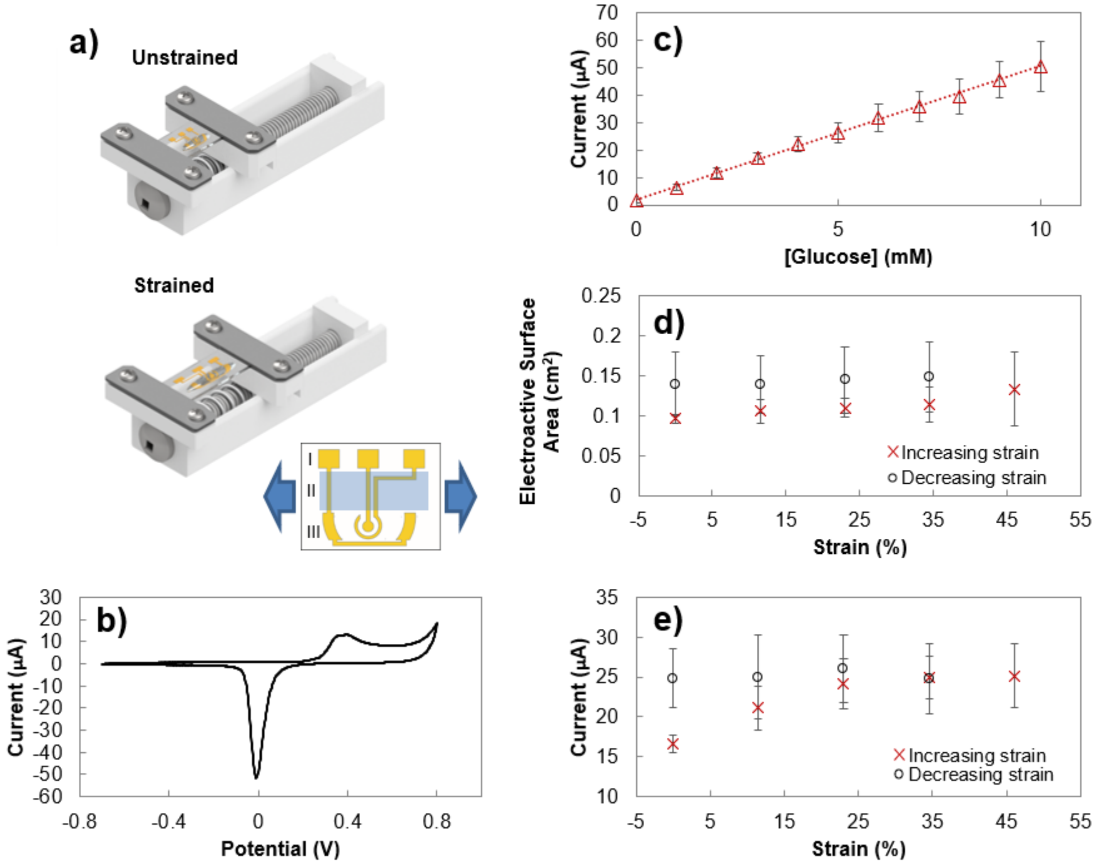

Figure 2.3. Electrochemical responses for on-chip electrochemical cell. (a) Illustration of the setup used for measuring electrochemical response under strain (strain direction indicated by blue arrows). (b) Cyclic voltammogram obtained using the on-chip electrochemical cell in 0.05 M H_2SO_4 at a scan rate of 0.1 V/s versus Ag/AgCl. (c) Calibration curve plotting current measured as a function of glucose concentration for on-chip electrochemical cell prior to stretching. (d) Electroactive surface area of the working electrode integrated on the on-chip electrochemical cell under strain. (e) Current measured as a function of strain for the glucose concentration of 5 mM glucose for on-chip electrochemical cell.

2.4.4 Resistance under strain

To understand the increasing current trend observed with small strains (≤ 25%), we investigated the sheet resistance *and* micro/nanostructure of the electrodes under strain. The resistance was measured using two different setups (Figure 2.4(a)). In the first setup, we placed the current measuring probes such that the current path was perpendicular to the direction of stretching. This measurement setup reflected the strain-current direction during the electrochemistry scans. In the second setup, the current path was designed to be parallel to the direction of stretching. In the perpendicular setup, the gold film was able to be strained up to 100% before failure and showed a consistently decreasing resistance as the strain was increased. In the parallel setup, the electrodes showed a stable resistance until approximately 30% strain was applied. After this threshold, the resistance increased until the electrodes were no longer conducting at a strain of 100%.

This significant difference in electrical characteristics when current flows perpendicular or parallel to the direction of strain was previously reported. Applying strain causes cracks to appear in the direction perpendicular to the strain [35], which was also observed in SEM images obtained under strain (Figure 2.4(b)). In the case where the strain and current path are parallel to each other, the propagation of cracks perpendicular to the current path increases the current path length and the resultant resistance [36]. This is not the case when the current path is parallel to the direction of the cracks. Additionally, when the substrate is strained, the wrinkles come into contact in the direction perpendicular to the strain (also observed in Figure 2.4(b)) and decrease the measured resistance in this direction [37]. This study demonstrates that the stretchable biosensors developed here work reliably up to a strain of 100% or 30% when the sensor is strained perpendicular or parallel to the current path respectively. This indicates that the design of electrode *configuration,* in addition to electrode material, is of paramount importance when creating stretchable biosensing platforms.

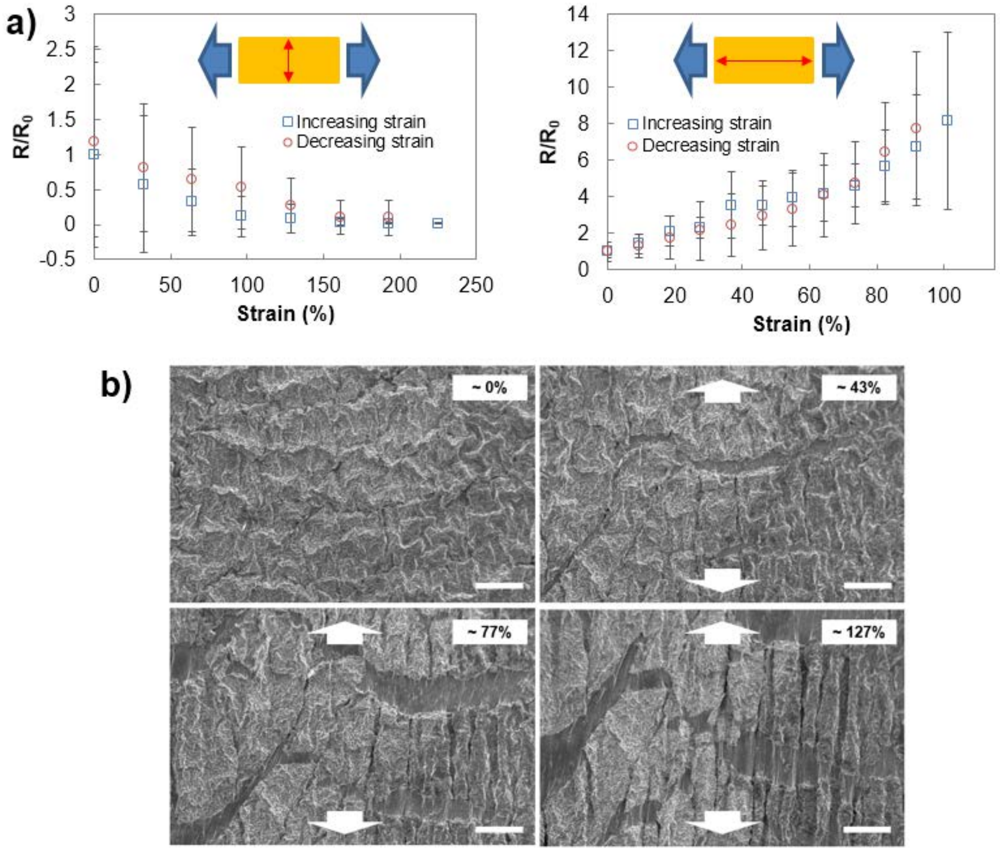

Figure 2.4. Resistance study of stretchable electrodes. (a) Relative resistance of wrinkled gold film on Ecoflex strained to failure and released. Direction of current measured is indicated by double sided arrow (red) and strain direction is indicated by the two larger arrows (blue). (b) SEM images of surface of gold film on Ecoflex under different strain. Direction of strain is indicated by the white arrows. Scale bar is 100 µm.

2.5 Conclusion

We demonstrated the fabrication of stretchable wrinkled electrodes for applying electrochemical readout to wearable biosensing systems. Previous work showed that wrinkled electrodes enhance the performance of biosensors by enhancing their analytical sensitivity [23] and increasing their detectible electrochemical current [21]. Here, we demonstrate that it is possible to create *stretchable* wrinkled electrochemical biosensors using a facile fabrication method based on solution-processing. It was found that transferring the wrinkled electrodes from rigid substrates to stretchable elastomers does not significantly alter their electrochemical behaviour, electroactive surface area, and analytical sensitivity. The stretchable biosensor created here showed an analytical sensitivity of 860 $\mu A/M.cm^2$ for detecting glucose, which is amongst the highest reported using gold electrodes [23,38]. It is found that the sensor shows dramatically improved strain resilience when it is stretched in a direction perpendicular to the current path compared to straining parallel to the current direction. Finally, these highly sensitive wrinkled biosensors can be strained by 100% in the direction perpendicular to the current path without significant loss in conductivity.

2.6 Experimental section

Reagents. Potassium chloride (KCl, ≥99.0%), (3-Aminopropyl)triethoxysilane (99%), Gold (III) Chloride solution (99%) and Toluene (≥99.5%) were purchased from Sigma-Aldrich (Oakville, Ontario). Ethanol (anhydrous) was purchased from Commercial Alchohols (Brampton, Ontario). Hydrogen Peroxide (30%) was purchased from Fisher

Scientific. Sulfuric acid (H_2SO_4, 98%), dextrose (CH2OH(CHOH)4CHO, >99%), and acetone was purchased from Caledon (Georgetown, Ontario). Sodium hydroxide (NaOH, 1.0 M) was purchased from LabChem (Zelienople, PA). All reagents were of analytical grade. Milli-Q grade water (18.2 MΩ) was used to prepare all solutions.

Polystyrene substrates preparation. Polystyrene substrates were prepared as described in a previous paper [23], with the silanization duration reduced to 2 hours. Vinyl was cut into the designed shape using the Robo Pro CE5000- 40-CRP cutter (Graphtec America Inc., Irvine, CA). The Polystyrene substrates were covered with a vinyl mask, fixed on petri dishes using double sided tape and submerged in a solution of gold nanoparticles overnight. Gold nanoparticles were synthesized as described previously. [39] The polystyrene substrates were rinsed with water and dried. Electroless deposition, as described in previously [23], was done for 20 minutes on the polystyrene substrates. After removing vinyl masks, the polystyrene substrates were placed in an oven (ED56 Binder, Tuttlingen, Germany) at 140°C for 5 minutes.

Electrodes transfer. The shrunken polystyrene substrates were submerged in animosilane bath (10% (3-Aminopropyl)triethoxysilane) for 2 hours. The aminosilane improved the bond between the Ecoflex and wrinkled gold surface as it works as a molecular adhesive [40]. Afterwards, the polystyrene substrates were rinsed and dried. Part A and part B of the Ecoflex (Ecoflex 0030, Sooth-On, PA) were mixed in a 1:1 ratio as outlined by the manufacturer. The mixture was poured over the polystyrene substrates and placed in a desiccator for 10 minutes. After 4 hours of curing, the Ecoflex enveloped polystyrene were placed in the oven at 80°C for 2 hours, followed by 100°C for another hour. The Ecoflex on the side of the electrodes was sliced off such that the polystyrene was exposed. The electrodes were placed in an acetone bath at 75°C for approximately 30 minutes. The electrodes were then rinsed and placed into a toluene bath at 65°C for approximately 15 minutes until all the polystyrene was dissolved. The electrodes were then placed on a glass slide to air dry.

Electroactive surface area. Electroactive surface area for polystyrene and Ecoflex electrodes were found by recording stable cycles of cyclic voltammetry in 0.05 M sulfuric acid at 0.05V/s scan rate. It was assumed that a monoatomic layer of oxygen was chemisorbed on the gold surface, and the amount of charge from the reduction of gold oxide was calculated by integrating the peak [41]. The resulting value was divided by the surface charge density of gold (386 μC/cm^2) to yield the electroactive surface area [42].

Electroactive surface area under strain. The on-chip electrochemical cells were strained by 11.5% increments and 10 CV scans were measured in a 0.05 M sulfuric acid solution between 0.7 V and +0.8 V at a scan rate of 0.1V/s. The same set of measurements were taken after the strain was released.

Glucose sensing. The sensitivity experiments were performed using chronoamperometry on the Reference 600 potentiostat (Gamry Instruments, Warminister, PA, USA). For polystyrene and Ecoflex electrodes, glucose concentrations from 1 to 10 mM were measured in a solution containing 0.1 M NaOH and 0.1 M KCl. Using pulsed amperometric detection, 0.8 V was applied to the electrode for 20 seconds for anodic cleaning, -0.6 V was applied for 20 s for cathodic regeneration, and 0.27 V or 0.35 V for 60 seconds for detection. Glucose was added in increments of 1 mM and mixed at 200 rpm on a shaker. The shaker was stopped during each detection step. The measured current over the first 5 seconds of the detection step was averaged, standardized by the electrode geometric surface area, and plotted as a function of the glucose concentration. The on-chip electrochemical cells were strained by 11.5% increments and a cycle of pulsed amperometric detection was performed. The same set of measurements were made while strain was released. The sensitivity of the electrode was found by taking the slope of the current versus concentration curve and dividing the slope by the geometric surface area.

Sheet resistance measurement. Sheet resistance was measured using the conventional four-point probe method with a sourcemeter (Keithley 2410). Sheet resistance of the material under strain was measured using the van der Pauw method with a square four-point probe configuration. Sheet resistances was calculated by assuming the sample is an infinite 2D sheet [43] as the thickness of the gold film was estimated to be approximately 55 nm [25].

Surface characterisation. SEM imaging was performed on a JEOL 7000F microscope. TEM imaging was performed on a JEOL 2010F microscope.

2.7 Acknowledgements

The financial support for this work was provided by the Natural Sciences and Engineering Council of Canada (NSERC) and Ontario Ministry of Research and Innovation. L.S is the Canada Research Chair in Miniaturized Biomedical Devices. The microscopy work was carried out at the Canadian Centre for Electron Microscopy, a facility supported by the Canada Foundation for Innovation under the Major Science Initiative program, NSERC, and McMaster University.

We would like to thank Jie Yang for her help with transmission electron microscopy (TEM) imaging and Marcia Reid for her help in cross-sectional TEM sample preparation.

2.8 References

1. Kim, D.-H., Ghaffari, R., Lu, N. & Rogers, J. A. Flexible and Stretchable Electronics for Biointegrated Devices. Annu. Rev. Biomed. Eng. 14, 113–128 (2012).

2. Patel, S., Park, H., Bonato, P., Chan, L. & Rodgers, M. A review of wearable sensors and systems with application in rehabilitation. J. NeuroEngineering Rehabil. 9, 21 (2012).

3. Yamada, T. et al. A stretchable carbon nanotube strain sensor for human-motion detection. Nat. Nanotechnol. 6, 296–301 (2011).

4. Amjadi, M., Pichitpajongkit, A., Lee, S., Ryu, S. & Park, I. Highly Stretchable and Sensitive Strain Sensor Based on Silver Nanowire–Elastomer Nanocomposite. ACS Nano 8, 5154–5163 (2014).

5. Roh, E., Hwang, B.-U., Kim, D., Kim, B.-Y. & Lee, N.-E. Stretchable, Transparent, Ultrasensitive, and Patchable Strain Sensor for Human–Machine Interfaces Comprising a Nanohybrid of Carbon Nanotubes and Conductive Elastomers. ACS Nano 9, 6252–6261 (2015).

6. Xu, F. & Zhu, Y. Highly Conductive and Stretchable Silver Nanowire Conductors. Adv. Mater. 24, 5117–5122 (2012).

7. Kim, J. et al. Highly stretchable wrinkled gold thin film wires. Appl. Phys. Lett. 108, 061901 (2016).

8. Wang, X., Hu, H., Shen, Y., Zhou, X. & Zheng, Z. Stretchable Conductors with Ultrahigh Tensile Strain and Stable Metallic Conductance Enabled by Prestrained Polyelectrolyte Nanoplatforms. Adv. Mater. 23, 3090–3094 (2011).

9. Zhao, S. et al. Recent Advancements in Flexible and Stretchable Electrodes for Electromechanical Sensors: Strategies, Materials, and Features. ACS Appl. Mater. Interfaces 9, 12147–12164 (2017).

10. Rogers, J. A., Someya, T. & Huang, Y. Materials and Mechanics for Stretchable Electronics. Science 327, 1603–1607 (2010).

11. Yoon, Y. et al. Highly Stretchable and Conductive Silver Nanoparticle Embedded Graphene Flake Electrode Prepared by In situ Dual Reduction Reaction. Sci. Rep. 5, (2015).

12. Yao, S. & Zhu, Y. Wearable multifunctional sensors using printed stretchable conductors made of silver nanowires. Nanoscale 6, 2345–2352 (2014).

13. Paek, J. et al. Stretchable electronic devices using graphene and its hybrid nanostructures. FlatChem 3, 71–91 (2017).

14. Zhang, H. et al. Piezoresistive Sensor with High Elasticity Based on 3D Hybrid Network of Sponge@CNTs@Ag NPs. ACS Appl. Mater. Interfaces 8, 22374–22381 (2016).

15. Mu, J. et al. An Elastic Transparent Conductor Based on Hierarchically Wrinkled Reduced Graphene Oxide for Artificial Muscles and Sensors. Adv. Mater. 28, 9491–9497 (2016).

16. Xu, F., Lu, W. & Zhu, Y. Controlled 3D Buckling of Silicon Nanowires for Stretchable Electronics. ACS Nano 5, 672–678 (2011).

17. Yu, Y. et al. Three-Dimensional Compressible and Stretchable Conductive Composites. Adv. Mater. 26, 810–815 (2014).

18. Li, X. et al. Multifunctional graphene woven fabrics. Sci. Rep. 2, 395 (2012).

19. Zhu, Y. & Moran-Mirabal, J. Highly Bendable and Stretchable Electrodes Based on Micro/Nanostructured Gold Films for Flexible Sensors and Electronics. Adv. Electron. Mater. 2, 1500345 (2016).

20. Park, S.-J., Kim, J., Chu, M. & Khine, M. Highly Flexible Wrinkled Carbon Nanotube Thin Film Strain Sensor to Monitor Human Movement. Adv. Mater. Technol. 1, 1600053 (2016).

21. Woo, S. M., Gabardo, C. M. & Soleymani, L. Prototyping of Wrinkled Nano-/Microstructured Electrodes for Electrochemical DNA Detection. Anal. Chem. 86, 12341–12347 (2014).

22. Gabardo, C. M., Zhu, Y., Soleymani, L. & Moran-Mirabal, J. M. Bench-Top Fabrication of Hierarchically Structured High-Surface-Area Electrodes. Adv. Funct. Mater. 23, 3030–3039 (2013).

23. Adams-McGavin, R. C. et al. Nanoporous and wrinkled electrodes enhance the sensitivity of glucose biosensors. Electrochimica Acta 242, 1–9 (2017).

24. Sargent, E. H. Infrared photovoltaics made by solution processing. Nat. Photonics 3, 325–331 (2009).

25. Gabardo, C. M. et al. Rapid prototyping of all-solution-processed multi-lengthscale electrodes using polymer-induced thin film wrinkling. Sci. Rep. 7, 42543 (2017).

26. Chen, C.-S. et al. Shrinky-Dink microfluidics: 3D polystyrene chips. Lab. Chip 8, 622 (2008).

27. Gabardo, C. M., Yang, J., Smith, N. J., Adams-McGavin, R. C. & Soleymani, L. Programmable Wrinkling of Self-Assembled Nanoparticle Films on Shape Memory Polymers. ACS Nano 10, 8829–8836 (2016).

28. Gabardo, C. M., Adams-McGavin, R. C., Vanderfleet, O. M. & Soleymani, L. Rapid prototyping of microfluidic devices with integrated wrinkled gold micro-/nano textured electrodes for electrochemical analysis. The Analyst 140, 5781–5788 (2015).

29. Tuomainen, T. P. et al. Body iron stores are associated with serum insulin and blood glucose concentrations. Population study in 1,013 eastern Finnish men. Diabetes Care 20, 426–8 (1997).

30. Egi, M. et al. Blood glucose concentration and outcome of critical illness: The impact of diabetes*. Crit. Care Med. 36, 2249–2255 (2008).

31. Rocklin, R. D., Clarke, A. P. & Weitzhandler, M. Improved Long-Term Reproducibility for Pulsed Amperometric Detection of Carbohydrates via a New Quadruple-Potential Waveform. Anal. Chem. 70, 1496–1501 (1998).

32. Austin-Harrison, D. S. & Johnson, D. C. Pulsed amperometric detection based on direct and indirect anodic reactions: A review. Electroanalysis 1, 189–197 (1989).

33. Johnson, D. C. & LaCourse, W. R. Liquid chromatography with pulsed electrochemical detection at gold and platinum electrodes. Anal. Chem. 62, 589A-597A (1990).

34. Chen, J.-C. et al. A disposable single-use electrochemical sensor for the detection of uric acid in human whole blood. Sens. Actuators B Chem. 110, 364–369 (2005).

35. Liu, N. et al. Ultratransparent and stretchable graphene electrodes. Sci. Adv. 3, e1700159 (2017).

36. Lee, J. et al. A stretchable strain sensor based on a metal nanoparticle thin film for human motion detection. Nanoscale 6, 11932–11939 (2014).

37. Liu, Z. F. et al. Hierarchically buckled sheath-core fibers for superelastic electronics, sensors, and muscles. Science 349, 400–404 (2015).

38. Wang, G. et al. Non-enzymatic electrochemical sensing of glucose. Microchim. Acta 180, 161–186 (2013).

39. Grabar, K. C., Freeman, R. G., Hommer, M. B. & Natan, M. J. Preparation and Characterization of Au Colloid Monolayers. Anal. Chem. 67, 735–743 (1995).

40. Byun, I., Coleman, A. W. & Kim, B. Transfer of thin Au films to polydimethylsiloxane (PDMS) with reliable bonding using (3-mercaptopropyl)trimethoxysilane (MPTMS) as a molecular adhesive. J. Micromechanics Microengineering 23, 085016 (2013).

41. Trasatti, S. & Petrii, O. A. Real surface area measurements in electrochemistry. Pure Appl. Chem. 63, (1991).

42. Cheng, T.-M. et al. (110)-Exposed Gold Nanocoral Electrode as Low Onset Potential Selective Glucose Sensor. ACS Appl. Mater. Interfaces 2, 2773–2780 (2010).

43. Miccoli, I., Edler, F., Pfnür, H. & Tegenkamp, C. The 100th anniversary of the four-point probe technique: the role of probe geometries in isotropic and anisotropic systems. J. Phys. Condens. Matter 27, 223201 (2015).

Chapter 3

Omniphobicity

3.1 Chapter introduction

This chapter detailed the fabrication of surfaces with nano-structures, micro-structures and a combination of both. The surfaces were tested for hydrophobicity, oleophobicity and for specifically for hierarchical structures, water droplet sliding angle and repellence towards blood. The various objectives for the thesis are addressed here.

Objective 1: Here, a process that takes less than three days to create are introduced. More than ten samples can also be done using the process in one batch. Specifically, the process includes using 4 minutes UVO treatment on polystyrene, all-solution process for depositing aminosilane, nanoparticles and fluorosilane onto the surfaces and thermal treatment for shrinking. The UVO treatment on pre-strain polystyrene provides an easy way to create wrinkled surfaces that can be easily functionalised through solution-based procedure. Through the processes, surfaces that are micro-structured (wrinkles), nano-structured (nanoparticles) and hierarchical structured (wrinkles with nanoparticles) were fabricated. The nanoparticles used are 12 nm gold nanoparticles (AuNPs) and 22 nm silica nanoparticles (SiNPs). The method provides easily controllable and achievable parameters.

Objective 2: The various surfaces' viability towards water and oil repellence were tested through water and hexadecane contact angle measurements. The measured water and hexadecane contact angles are 125±4° and 26±7° (wrinkled surfaces), 132±2° and 69±6° (AuNPs surfaces), 135±4° and 55±3° (SiNPs surfaces), 151±2° and 116±3° (wrinkled AuNPs surfaces) and 155±2° and 123±5° (wrinkled SiNPs surfaces) respectively. The results demonstrated that the hierarchical structures did the best for both high and low surface tension liquid. It also indicated that wrinkles are more oleophilic than nanoparticles surfaces. The nanoparticles provide re-entrant texture and the wrinkles increase roughness. In addition, the hierarchical surfaces also allow sliding of water droplet at 15±4° (wrinkled AuNPs surfaces) and 8±7° (SiNPs surfaces).

Objective 3: Lastly, the wrinkled AuNPs and wrinkled SiNPs surfaces were examined for their blood repellence though contact angle (138±3° and 142±7° respectively) and adhesion (reduction of ~90% compared to untreated polystyrene) tests. It was shown conclusively that the omniphobic surfaces (wrinkles and nanoparticles) work well to reduce blood adhesion, showing the potential of using such surfaces for medical devices.

As reproduced from the preface, the second paper consisted of contributions from Sara Imani and Kenneth Rachwalski. Kenneth, with Sara, assisted with collection of data for bacteria adhesion. Sara assisted with collection of data for contact angle measurements for blood and adhesion for blood and bacteria. She also contributed in writing for the analysis of these data. The writing of the rest of the manuscript was done by the author. Dr. Soleymani assisted with helpful suggestions and revision of the manuscript.

Omniphobic surfaces with hierarchical structures incorporating wrinkles and nanoparticles

Yutting Chan [a], Sara Imani[b], Kenneth Rachwalski [c], Eric Brown [c,d], Tohid F. Didar [b,d,e], Leyla Soleymani [a,b,*]

[a] Department of Engineering Physics, McMaster University, 1280 Main Street West, Hamilton, ON L8S 4L7, Canada
[b] School of Biomedical Engineering, McMaster University, 1280 Main Street West, Hamilton, ON L8S 4L7, Canada
[c] Department of Biochemistry and Biomedical Sciences, McMaster University, 1280 Main Street West, Hamilton, ON L8N 3Z5, Canada
[d] Michael G. DeGroote Institute of Infectious Disease Research, McMaster University, 1280 Main Street West, Hamilton, ON L8N 3Z5, Canada
[e] Department of Mechanical Engineering, McMaster University, 1280 Main Street West, Hamilton, ON L8S 4L8, Canada
* Corresponding author. E-mail address: soleyml@mcmaster.ca (L. Soleymani)

3.2 Abstract

Omniphobic surfaces are useful for applications that require repellence to either low or high surface tension liquid. One such application is medical devices where resistance to fouling by blood is important. A major strategy for achieving omniphobic surfaces is through creation of hierarchical structures. One of the major challenges is finding a facile and scalable fabrication method. Here, we proposed a procedure that made use of the spontaneous and self-organizing buckling process together with all solution-based depositions to create wrinkled surfaces decorated with nanoparticles. These surfaces achieved the water contact angle of 155±2°, hexadecane contact angle of 123±5°. The omniphobic surface demonstrated low adhesion to water (8 ± 7° sliding angle) and blood.

3.3 Introduction

Omniphobicity had been an intense subject of study to create surfaces that are self-cleaning [1,2], anti-icing [3,4] and anti-fouling [5,6]. These surfaces are important for applications such as aircrafts, marine vessels, automobile, medical devices or microfluidic devices where water and oil repellence are valuable properties.

In-depth studies had been done both experimentally and theoretically to show that a rough surface texture is necessary to achieve high hydrophobicity [7–12] and it had been reported that hierarchical structures with re-entrant texture are the ideal model for robust omniphobic surfaces [13,14]. In addition to hierarchical structures, another approach to achieve enhanced repellency is through slippery liquid infused porous surfaces (SLIPS), which are stable under high pressure and have extremely low adhesion with no dependence to surface tension of liquid [15]. However, because SLIPS depend on the infusing of lubricant into porous substrate, continuous flow of fluid can wick away the capillary trapped lubricant [16] affecting its performance detrimentally. Such lubricant also blocks surface sites, reduce biofunctionalization ability and increase difficulty for patterning surfaces for different functionalities. As such, hierarchical structures with low surface energy coating are the focus of our work.

The fabrication of such omniphobic artificial hierarchical surfaces are generally rather complex [17]. They range from the simpler emulsion templating [18], electrospinning onto surfaces [19] to the more complex electrochemical etching/anodizing [20], reactive ion etching [21] or conventional photo-lithography [19]. The formation of wrinkles is a spontaneous process with features that can range from nanometres to micrometres [22–24], which provides a competitive alternative to the simpler methods. It also addresses one of the challenges for commercialising omniphobic surfaces which is finding a fabrication method suitable for large scale production [17].

Some of the highest contact angle values achieved for hierarchical structures are 172° for water (nano-pillars and branching structures) [21] and 156° (fractal-like structures from soot) [25] or 174° (string-like structures) [26] for hexadecane. It was shown that structures improve water contact angles measured along ripples in this sequence [12]: flat (112°), micro-scale uniaxial ripples (124°), nanoparticle film (128°) and nanoparticles on uniaxial ripples (150°). These microscale ripples of approximately 2 μm to 4 μm wavelength, were formed by release of 40% pre-strained polydimethylsiloxane. The compression of ultraviolet-ozone (UVO) treated polystyrene by 60% strain in two dimensions generates more complex morphology of wrinkles (0-1 μm) mixed with folds. Compared to ripples, such complex morphology is more analogous to fractal-like soot structure. In combination with nanoparticles, it can be expected that this type of structures results in re-entrant textures that are not only expected to be hydrophobic, but also oleophobic.

Due to the requirement of oil repellence for most applications, studies involving oleophobicity of surfaces are becoming increasing important. In particular, blood has a surface tension of approximately 55 mJ/m^2 [27], and increasing oil leakage accidents can cause marine biofouling of oceanographic sensors [28]. Both relate to lower surface tension liquid than water. However, for wrinkled structures formed via compression of substrates, previous papers had only focused on its impact on hydrophobicity [29–34], achieving the high water contact angle of 172° [29].

In this work, we explored the wettability impact of micro-structures (wrinkles) and nano-structures (nanoparticles) both separately and in combination. This provides relevant insights for designing surfaces that are repellent to both water and other complex liquid. Lastly, we tested the surfaces' repellence to blood to show their potential for use in applications relating to medical devices.

3.4 Results and discussion

3.4.1 Combination of wrinkles and nanoparticles for different surfaces

We designed processes (Figure 3.1) to create substrates decorated with micro-structures (wrinkles), nano-structures (nanoparticles) and hierarchical structures (wrinkles with nanoparticles) treated with fluorosilane coating. The fluorosilane is a common chemical used for lowering surface energy [35] which is a common method for increasing repellency of surfaces.

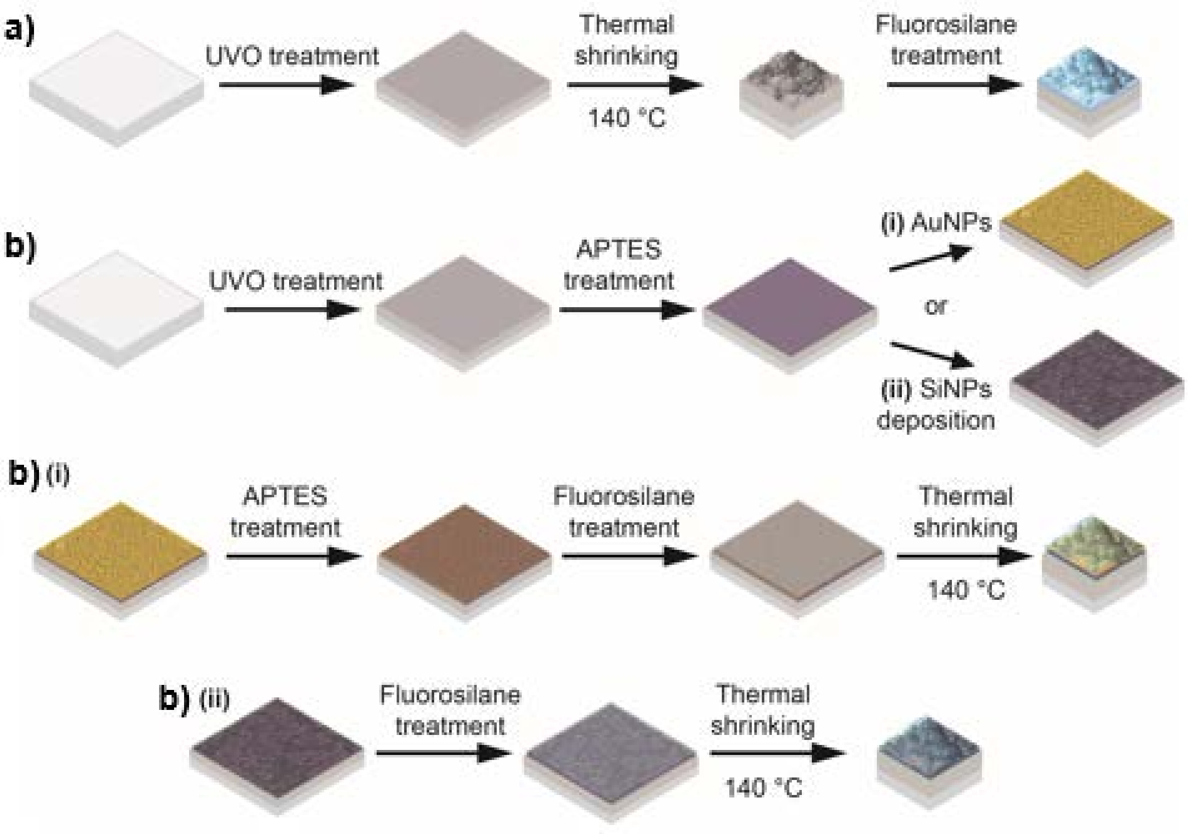

Figure 3.1.Schematic illustrating processes for fabrication of the different surfaces for contact angle testing. (a) Processes for creating a wrinkled surface. (b) Processes for creating surfaces with nanoparticles (b)(i-ii) Processes for creating wrinkled surfaces with nanoparticles.

The first step for creating micro-structures on surfaces consists of activating a pre-strained polystyrene substrate through Ultraviolet-Ozone (UVO) treatment. After which, through thermal treatment, the substrates were shrunk. The stiffness differential due to the UVO treatment resulted in a buckling of the surface into wrinkles after compression. Using the hydroxyl groups introduced to the surface due to the previous UVO treatment, fluorosilane was covalently bonded onto the surface through hydrolysis and condensation reactions [36].

To create nanostructures on surfaces, the UVO treated substrates were coated with aminosilane molecular linker layer. The layer allowed the deposition of 12 nm gold nanoparticle (AuNPs) solution or 22 nm colloidal silica (SiNPs) as the amine terminus on aminosilane had electrostatic interactions with the citrate surfactant of AuNPs [37] and the negative surface charge of the SiNPs. An additional layer of aminosilane on the AuNPs decorated substrates allowed deposition of the final layer of fluorosilane. For polystyrene decorated with SiNPs, aminosilane was not required as the hydroxyl groups on the SiNPs enable direct deposition of fluorosilane.

Finally, to create hierarchical structures, the fluorinated nanoparticles decorated substrates were shrunk through thermal treatment. In addition to these surfaces, we also included non-fluorinated surfaces with and without wrinkles: untreated polystyrene, shrunken polystyrene and shrunken 4 min UVO treated polystyrene as a control group. These morphologies were examined through scanning electron microscope (SEM) images (Figure 3.2 column 2). These images confirmed the fabrication of wrinkled surfaces (structures of micrometre scale), nanoparticle surfaces (structures of nanometre scale) and wrinkled surfaces with nanoparticles. Using these different surfaces, we investigated the effect of having hierarchical structures on omniphobicity.

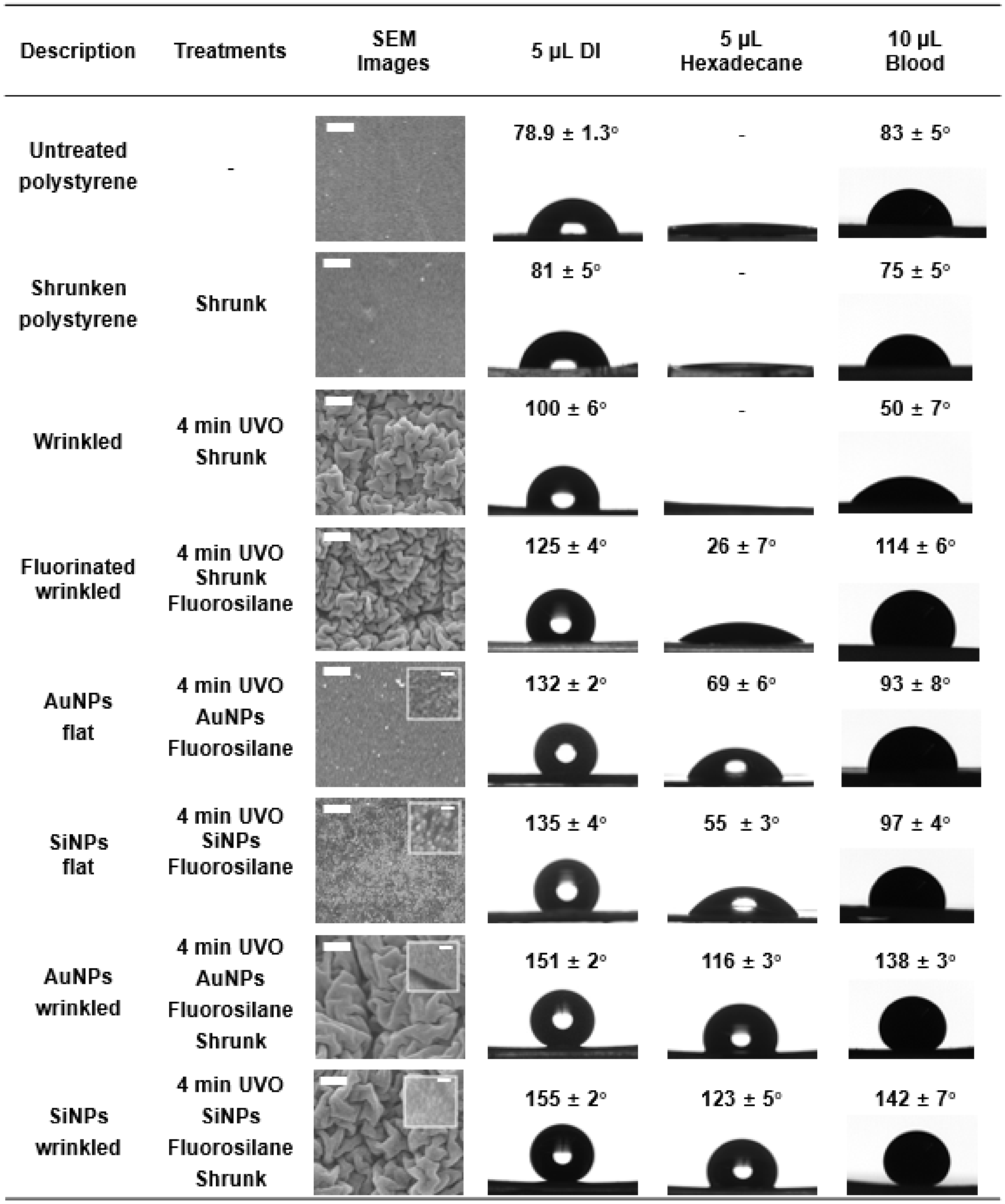

Description	Treatments	SEM Images	5 µL DI	5 µL Hexadecane	10 µL Blood
Untreated polystyrene	-		78.9 ± 1.3°	-	83 ± 5°
Shrunken polystyrene	Shrunk		81 ± 5°	-	75 ± 5°
Wrinkled	4 min UVO Shrunk		100 ± 6°	-	50 ± 7°
Fluorinated wrinkled	4 min UVO Shrunk Fluorosilane		125 ± 4°	26 ± 7°	114 ± 6°
AuNPs flat	4 min UVO AuNPs Fluorosilane		132 ± 2°	69 ± 6°	93 ± 8°
SiNPs flat	4 min UVO SiNPs Fluorosilane		135 ± 4°	55 ± 3°	97 ± 4°
AuNPs wrinkled	4 min UVO AuNPs Fluorosilane Shrunk		151 ± 2°	116 ± 3°	138 ± 3°
SiNPs wrinkled	4 min UVO SiNPs Fluorosilane Shrunk		155 ± 2°	123 ± 5°	142 ± 7°

Figure 3.2. Tabulated data listing SEM images and static contact angle measurements for different liquid on various surfaces. The main SEM images' scale bars are 1 µm and the insets' scale bars are 100 nm.

The study of the wettability of a surface towards different liquid starts with the examination of the contact angle of sessile droplets placed on the surface. An omniphobic surface would demonstrate high contact angle (>90°) for both high surface tension (water) and low surface tension liquid (hexadecane), known as hydrophobic and oleophobic surfaces respectively. Previous literature involving wrinkles had achieved water contact angle of 172° [29]. For wrinkled surfaces from buckling of surfaces, to the best of the author's knowledge, there was no studies on its repellence to oil. Other hierarchical structures, however, were able to achieve 156° [25] or 174° [26] for hexadecane. There are limitations to some of the surfaces proposed due to how the structures were engineered. Some examples are etching (electrochemical [20] or reactive ion [21]) to achieve nanopillars, photolithography [19] or templating using soot [25,38]. The first two methods are complex, requiring precisely controlled parameters, and the third, difficult to scale. Another example requires the use of toluene [26], a solvent, which limits the use of polymer as a substrate. Some other surfaces used spraying coating [39] and dip coating [40]. Our all-solution based and wrinkling method is competitive with these, with its simple to control parameters. Here, we will first examine the fabricated surfaces' repellence to water and follow up with low surface tension liquid and more complex liquid.

3.4.2 Assessment of hydrophobicity of surfaces

Static contact angle measurements were made for 5 µL droplets of milli-Q grade water (surface tension of 72.75 mJ/m^2 [41]) deposited onto the surfaces (Figure 3.2). The non-fluorinated surfaces were shown to be hydrophilic with contact angles of approximately

80°. Non-fluorinated wrinkled surfaces were hydrophobic, showing a contact angle (~100°) higher than 90°. Based on the Wenzel model [8], for a fully wetted state between the droplet and surface, the apparent contact angle can be estimated by [8],

$$\cos\theta_w = r\cos\theta \ , \tag{12}$$

where r is the ratio of the actual surface area in contact with the droplet to the projected surface area of the droplet and θ is the contact angle based on Young's relation. This equation indicates that a rough surface, with fully wetted state, would result in a lower Wenzel contact angle for $\theta < 90°$ and higher Wenzel contact angle for $\theta > 90°$. Based on this, as the non-fluorinate flat surfaces are hydrophilic ($\theta < 90°$), we can reasonably assume that the water droplet on the wrinkled surface did not fully wet the surface and was better described by the Cassie model [9]. The contact angle for a such a droplet, θ_C, can be estimated as [9,13,42],

$$\cos\theta_C = f_{SL}\cos\theta + f_{LV}\cos\pi = f_{SL}\cos\theta - f_{LV} \tag{13}$$

where f_{SL} is the ratio of the total area of solid-liquid interface to the projected area of the drop and f_{LV} is the ratio of the liquid-air interface to the projected area of the drop. This enables prediction of a higher Cassie contact angle due to fraction of liquid-air interface beneath the droplet regardless of the starting Young's contact angle.

The fluorinated wrinkled surfaces had higher contact angle (~125°). This is explained by the lowering of the surface free energy which results in a higher Young's contact angle and leads to a higher Cassie contact angle. The surfaces with fluorinated nanoparticles had similar repellence towards water (AuNPs: ~132°, SiNPs: ~135°). For closed packed nanoparticles, the surface area in contact with the droplet can be approximated to be the same for different sizes, similar with the roughness approximation done for the Wenzel model of hemispherical close-packed model [43]. This means that the contact angle should not be affected regardless of the sizes of the nanoparticles. This was observed in previous papers for close packed nanoparticles [44,45]. The contact angle measured for the two surfaces were within standard deviation, showing good consistency with expectation. Based on the contact angle results, the nanoparticles (~132-135°) had higher repellency towards water than wrinkles (~125°).

The combination of both micro- and nano-structures on the surface achieved hydrophobicity of more than 150°. For hierarchical structures, the contact angle can be approximated theoretically by rewriting Cassie relation recursively [46],

$$\cos\theta_{c,n} = \left(1 - f_{LV,n}\right)\cos\theta_{c,n-1} - f_{LV,n} \tag{14}$$

where $n = 1, 2, 3, \ldots$ corresponding to the number of length scale of texture, with larger n corresponding to larger length scale. This means that the contact angle is expected to increase as the number of length scale increases [13]. It had also been shown in a previous study that multiscale roughness assists to improve the stability of solid-liquid-air interface [10]. Here, we demonstrated that having a combination of both nanoscale and microscale structures improved the hydrophobicity by approximately 20°.

3.4.3 Assessment of oleophobicity of surfaces

For our surfaces, to test for oleophobicity, 5 μL droplets of hexadecane (surface tension of 27.76 mJ/m^2 [41]) was deposited onto the surfaces and their static contact angles measured (Figure 3.2 column 3). The non-fluorinated surfaces performed badly for hexadecane, with contact angles that are too low to be accurately measured. This was as expected since the Young's relation predicts a smaller contact angle for lower surface tension liquid. The inclusion of non-fluorinated wrinkles on surfaces also does not assist in making the surface less oleophilic. Fluorinated wrinkles made the surface less oleophilic (~26°). This is similar with the effect of fluorinated surface on water because of its lower surface energy.

The nanoparticles decorated surfaces resulted in a significantly higher contact angles (AuNPs - ~69°, SiNPs - ~55°). The AuNPs and SiNPs surfaces were more effective when compared to wrinkled surfaces for improving the contact angle for hexadecane than water. This could be explained by the re-entrant texture of nanoparticles compared to that of wrinkles. The wrinkles were not effective for keeping lower surface tension liquid in the Cassie state. In a Cassie state, when pockets of air are trapped beneath the droplet, the liquid forms a three-phase contact line at the local structure (Figure 3.3a), where the local geometric angle, ψ, becomes equal to the equilibrium contact angle, θ, based on Young's relation [13]. The structure of a wrinkle is similar with that of a concave texture where the local geometric angle has a high value, $\psi > 90°$. Previous studies had concluded that concave structure does not support a stable Cassie state [13,47]. For a stable Cassie state, the Young's contact angle must be higher than the local geometric angle [13] and Young's relation equilibrium contact angle decreases for lower surface tension liquid. When the angle decreases to below the local geometric angle, the net traction on the liquid-air interface is downwards due to capillary forces [13,19], which will lead to a fully wetted Wenzel state. For local geometric angles of high values, such as for wrinkles, the surface tension of the liquid needs to be high for a stable Cassie state.

The combination of both micro- and nano-structures on the surface achieved oleophobicity (wrinkled AuNPs - ~116°, wrinkled SiNPs - ~123°). The addition of nanoparticles decreased the limitation of the concave texture of the wrinkles, allowing better repellence of lower surface tension liquid. In the meantime, having wrinkles also provided for a higher fraction of air beneath the droplet. The results showed that the surfaces created are omniphobic, with oleophobicity (>110°) and hydrophobicity (>150°).

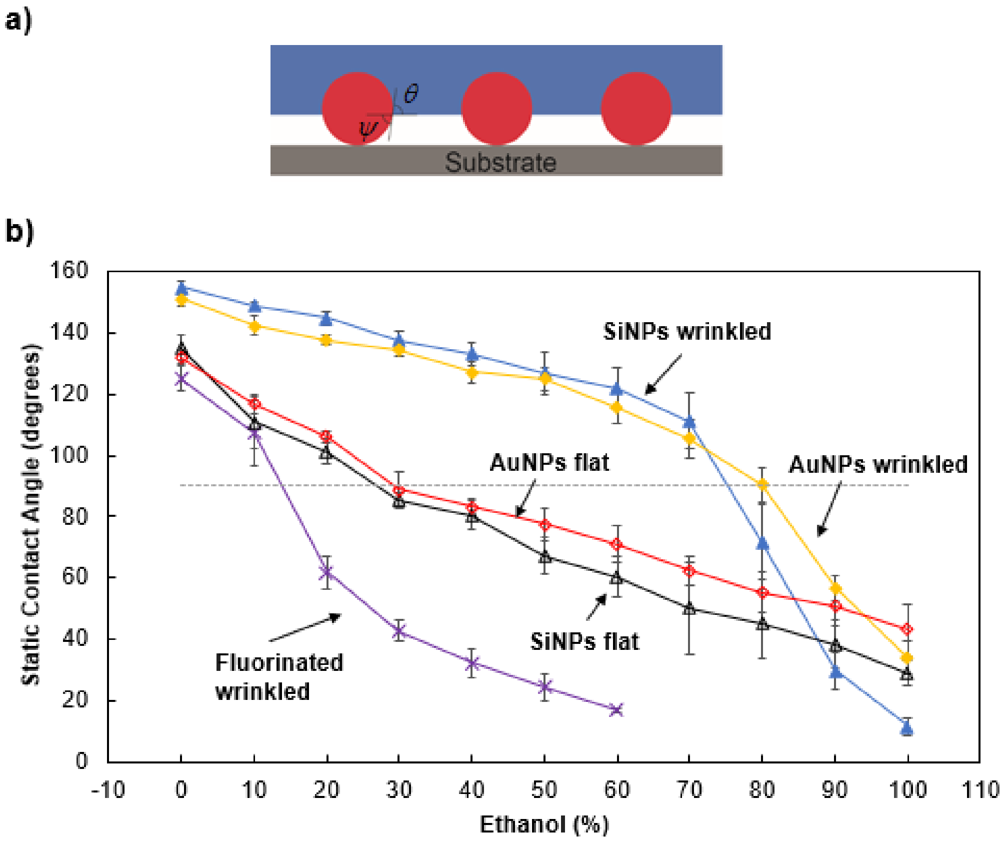

Figure 3.3. Study of omniphobicity of surfaces. (a) Illustration of the Cassie wetting of local texture with indication of local geometric angle, ψ , and the Young's contact angle, θ [13]. Adapted from paper [13]. (b) Graphical data representing the wetting characteristic of different surfaces for liquid with different surface tension through variation of ethanol content. The letters indicate the type of surfaces as tabulated in Figure 2.

It was previously shown that live B. subtilis biofilms provides a contact angle plateau (~135 to 145°) from 0 to 80% ethanol concentration compared to the relatively linear decrease (~135 to 60°) of an artificial replica [48]. To expand on the hexadecane tests, the fluorinated surfaces in this work were also tested with different ethanol content (Figure 3.3b). We found that the best performing surface is the wrinkled AuNPs surfaces, which maintained contact angle above 90° till 80% ethanol. The range of contact angle (~90 to 150° for wrinkled nanoparticles surfaces) from 0 to 80% ethanol did not provide a contact angle plateau and followed a linear trend till 70%. Regardless, the wrinkled nanoparticles surfaces did maintain phobicity (>90°) up to 70-80% ethanol.

The AuNPs surfaces were similar with SiNPs in their repellence to liquid of different surface tension while the wrinkled surface without any nanoparticles was the least effective, agreeing with earlier hexadecane contact angle results. For AuNPs and SiNPs surfaces both flat and wrinkled, the ethanol results imply a tendency for AuNPs to be more effective as surface tension decreases. The hexadecane measurement also indicated that the AuNPs flat surfaces were more effective than SiNPs flat surfaces. This may be due to the defects that appears to be more significant on the surfaces with SiNPs, as can be observed from the SEM images. The robustness factor [49] for Cassie state is expected to decrease due to the larger spacing between particles, leading more easily to fully wetted state and higher fraction of wetted surface area. This instability was accentuated for lower surface tension liquid. F/or wrinkled surfaces, the larger spacing caused by the defect was less pronounced due to shrinking, which resulted in better performance for wrinkled SiNPs surfaces for a larger range of surface tension.

3.4.4 Adhesive performance of hierarchical structures

Another important characteristic of omniphobicity is their low sliding angle. Having a low sliding angle is an essential property for self-cleaning surfaces [50] as it reflects the adhesiveness of the surfaces to liquid. We chose the surfaces with the highest contact angle values for the sliding angle tests. The sliding angles of 10 μL of milli-Q water droplets were measured for the wrinkled AuNPs and SiNPs surfaces. The measurements of 15 ± 4° (see Video 1) and 8 ± 7° (see Video 2) respectively demonstrated that there is low adhesion of water droplet for such surfaces. The ability of the droplet to slide off such hierarchical surface, shown by the <20° sliding angle, may be explained by the unevenness of the height of the wrinkles in combination with nanoparticles. We can observe the roughness of the morphology from the SEM images (Figure 3.2 column 2). This unevenness means that when the surface is tilted, the droplet only needs to detach itself sequentially with small areas, resulting in a smaller adhesive force [51]. The ability for water to slide off these surfaces will be useful in terms of self-cleaning, anti-fouling properties or transportation of microfluid.

3.4.5 Interaction of omniphobic hierarchical surfaces with blood

The surfaces were tested with heparinized whole human blood as a complex liquid, to further evaluate the omniphobic behaviour of surfaces and the potential use in blood contacting medical devices and implants. The behaviour of 10 μL droplet of blood on each surface was examined. Wrinkled AuNPs and SiNPs surfaces (micro- and nano-structured surfaces) maintained a high contact angle of 138±3° and 142±7°, respectively (Figure 3.2). The similar trend in blood contact angle was observed for other control groups as was observed for water (Figure 3.2).

The omniphobic surfaces along with the proper control groups were dipped in blood in order to allow for the blood to attach to each sample. The adhered blood to each surface was subsequently resuspended by adding water to wells containing a sample each and further agitated to transfer the adhered blood in solution in order to quantify the extent of blood adhesion to each surface. Figure 3.4a shows the relative absorbance of each well to the absorbance of untreated polystyrene for each sample as well as representative images of each well. The results reveal superior performance of surfaces with both micro- and nano-structures (relative values of 0.1 for wrinkled AuNPs and 0.07 for wrinkled SiNPs) which show more than 10 folds decrease in the relative absorbance than the non-fluorinated flat surfaces (untreated polystyrene – 1, shrunken polystyrene - 1). Furthermore, the fluorinated nano-structured surfaces and the micro-structured surface showed a reduced blood adhesion (AuNPs - 0.4, SiNPs - 0.4, and wrinkled - 0.6) comparing to untreated samples. However, the wrinkled AuNPs and wrinkled SiNP surfaces still showed a lower relative absorbance which is an indicative of less blood attached to their surfaces. Furthermore, samples were incubated in blood for 30 minutes to allow blood to adhere to the surfaces and subsequently, washed 2 times with water. As shown in Figure 3.4b, wrinkled AuNPs and wrinkled SiNPs surfaces have lower amount of blood adhered to them comparing to the untreated samples as well as the flat AuNPs, flat SiNPs, and fluorinated wrinkled samples.

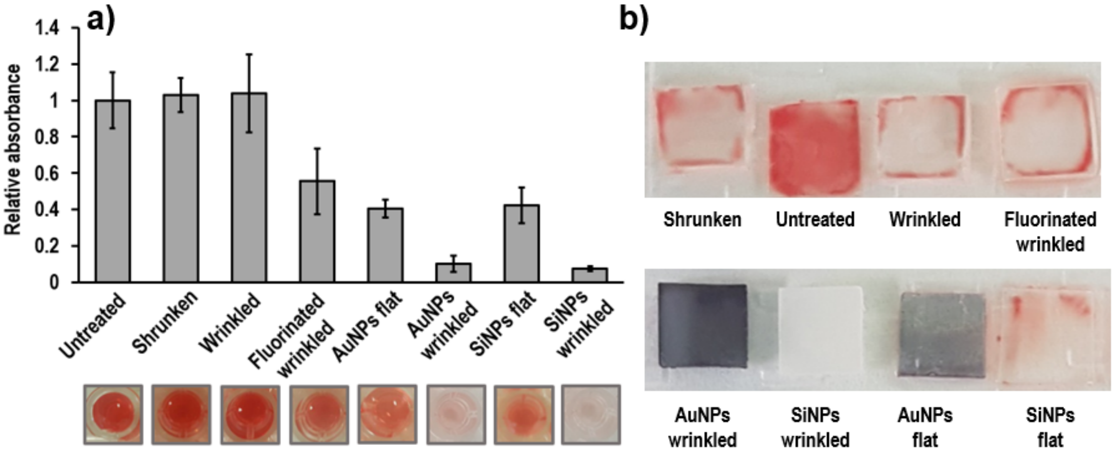

Figure 3.4. Study of blood adhrance to the omniphobic hierarchical surfaces. (a) Relative absorbance of resuspension of attached blood to each surface, to the absorbance of the resuspension of attached blood to untreated polystyrene for each sample. Representative images of each well is shown at the botton of the figure. (b) Representative images of samples which were incubated 30 minutes in blood after 2X wash.

3.4.6 Applications of fabricated hierarchical structured surfaces

The developed hierarchical structured surfaces were tested for application-relevant conditions, to seek potential of incorporating these surfaces in blood contacting devices or implants. It was demonstrated that having both nano- and micro-structures led to a higher contact angle and repellent characteristic when coming in contact with blood as shown in Figure 3.2 and Figure 3.4. As predicted by the contact angles, other samples showed more blood attached to their surfaces which led to a higher relevant absorbance value in the blood solution which correlates with the fact that more blood sticks to these surfaces. Also, incubation in blood and the subsequent washing showed that the omniphobic sample did not hold on to blood comparing the other control groups. These findings suggest that the omniphobic hierarchical surfaces effectively repels whole blood and can be promising candidates for being utilized in blood-contacting environments. Incorporation of nano-structures or micro-structures along with the fluorosilane treatment, showed an improved relative absorbance comparing the untreated samples which was assumable due to the lower contact angles that these surfaces had. Furthermore, comparing these surfaces to the hierarchical surfaces, in all cases, the hierarchical surfaces revealed a significant reduction in the amount of blood adherence.

In addition to the surfaces' potential for use in blood contacting devices, there are also other possibilities. Wrinkles had been proposed as ways to create biointerfaces with alignment of cells [52], for improving electrochemical sensing [53–55] and photovoltaic efficiency [56]. The ability for wrinkled structures to be omniphobic have great potential for patterning surfaces for selective functionalisation [57] on devices. Using vinyl patterning [53], the surface can be treated for different functionalities depending on requirements easily. The decrease in dimension due to shrinking also provides a way to miniaturize designs easily. This has potential for prototyping devices for different applications.

3.5 Conclusion

In this paper, we created surfaces with micro- and nano-structures utilizing wrinkles and nanoparticles that can be fabricated easily through bench-top equipment. As such, the procedure has simple to control parameters and is time and cost effective. These surfaces were characterised through SEM and the omniphobicity of the surfaces were studied through static contact angle measurements. We demonstrated that surfaces with only wrinkles were not as effective towards low surface tension liquid compared to surfaces with only nanoparticles (~26° compared to ~55°) even when they were both hydrophobic (~125° and ~132-135° respectively). Explanation for the behaviour was suggested by examining the Cassie and Wenzel models, indicating the limitations of the concave structure of wrinkles for low surface tension liquid. However, the hierarchical structures fabricated showed good performances for water (>150°) and oil repellence (>110° for hexadecane) and satisfactory performance for sliding angle for water (<20°). Even though the water contact angle and hexadecane contact angles are lower than previous achieved for wrinkled surface (172°) and hierarchical surface (156°), our work provides value by demonstrating that wrinkles with nanoparticles is a viable design for achieving better repellence of both water and oil. It was also the first work with wrinkled structure formed through buckling shown to be oleophobic/omniphobic. Finally, with the shown repellency to blood (>135°) and approximately 90% less adhesion compared to untreated surfaces, the hierarchical surfaces engineered can be useful for medical devices that requires such property.

3.6 Methods

Reagents. (3-Aminopropyl)triethoxysilane (99%), 1H,1H,2H,2H-Perfluorodecyltriethoxysilane (97%), Ludox® TMA colloidal silica were purchased from Sigma-Aldrich (Oakville, Ontario). Ethanol (anhydrous) was purchased from Commercial Alchohols (Brampton, Ontario). Hydrochloric acid (36.5–38%) was purchased from Caledon (Georgetown, Ontario). Milli-Q grade water (18.2 MΩ) was used to prepare all solutions.

Gold NPs Synthesis. AuNPs were synthesized according to protocol described previously (Preparation 1) [58] and were kept at 4°C until used.

Wrinkled Surfaces Fabrication. Pre-strained polystyrene (Graphix Shrink Film, Graphix, Maple Heights, Ohio) was cut into desired substrate sizes using Robo Pro CE5000-40-CRP cutter (Graphtec America Inc., Irvine, California). The polystyrene substrates were cleaned with ethanol, milli-Q water and dried with air. The substrates were placed in pre-warmed-up (5 minutes) UVO cleaner (UVOCS model T0606B, Montgomeryville, Pennsylvania) for the desired time.

For the deposition of fluorosilane, a mixture of ethanol and milli-Q water with volume ratio of 3:1 was prepared. A catalytic amount of Hydrochloride acid (0.1 wt%) was added into the solution with 0.5 wt% of fluorosilane. The solution was incubated at 40° for an hour before use.

The activated substrates were submerged in desired solution (10% aqueous APTES or prepared fluorosilane solution) for approximately 3 hours with agitation at room temperature in an incubating mini shaker (VWR International, Mississauga, Ontario). Following deposition of coating, the substrates were sonicated in Milli-Q water for 10 minutes and dried to remove 2 molecules.

SiNPs solution was created by vortexing 1-part Ludox TMA colloidal silica with 2-parts milli-Q water for 10 seconds and sonication for half an hour. For the deposition of AuNPs/SiNPs, the substrates were fixed in petri dishes using double sided tape and submerged in the AuNPs/SiNPs solution overnight. Following deposition, the substrates were sonicated in Milli-Q water for 10 minutes and dried.

To coat the AuNPs covered substrate with fluorosilane, the substrates were first submerged in 10% aqueous APTES for approximately 3 hours with agitation. The substrates were sonicated in milli-Q water for 10 minutes and dried. Following silanization of the AuNPs surface, the substrates were placed in the prepared fluorosilane solution for approximately 3 hours with agitation. The SiNPs surface were placed in the prepared fluorosilane solution for the same duration without silanization. The fluorosilane deposition is similar with a protocol used to create omniphobic micro- and nano-structured fabrics [59]. The substrates were then sonicated in milli-Q water for 10 minutes and dried.

Thermal treatment was performed by placing the substrates into an oven (ED56, Binder, Tuttlingen, Germany) pre-heated to 140°C for 5 minutes.

Wrinkled Surface Characterisation. SEM imaging was performed on a JEOL 7000F. Samples were coated with 3 nm of platinum prior to imaging. Contact angle measurement was made on a goniometer (OCA 20, Future Digital Scientific, Garden City, NY) with water droplets dispensed by automated syringe and other liquid by hand using pipette. The sessile drop contact angle was provided via image processing software (Dataphysics SCA 20) through ellipse curve fit shape analysis of the droplets. Sliding angle measurements were made on a self-made tilting platform with angle controlled by an automated servo. Each value was averaged over at least three measurements.

Whole human blood assays. Whole human blood was collected from healthy donors in BD heparinized tubes. All donors provided signed written consent and the procedures were approved by the McMaster University Research Ethics Board. Blood sessile drop contact angle was measured at room temperature using the goniometer. The extent of blood adherence was evaluated by dipping each sample in human whole blood and resuspending the adhered blood to each surface by transferring each substrate in a well and adding 700 μL of water. To ensure the adhered blood was transferred in solution, samples were placed on a shaker for 30 minutes. 200 μL of each well was transferred to a 96 well and the absorbance was measured at 450 nm wavelength on a SpectraMax plate reader. To ensure reproducibility, 6 samples per each condition was evaluated. Samples were also incubated in blood for 30 minutes and washed subsequently by dipping in water two times to evaluate the extent of stickiness of the surfaces.

3.7 References

1. Fürstner, R., Barthlott, W., Neinhuis, C. & Walzel, P. Wetting and Self-Cleaning Properties of Artificial Superhydrophobic Surfaces. *Langmuir* **21,** 956–961 (2005).

2. Parkin, I. P. & Palgrave, R. G. Self-cleaning coatings. *J. Mater. Chem.* **15,** 1689 (2005).

3. Wang, Y., Xue, J., Wang, Q., Chen, Q. & Ding, J. Verification of Icephobic/Anti-icing Properties of a Superhydrophobic Surface. *ACS Appl. Mater. Interfaces* **5,** 3370–3381 (2013).

4. Cao, L., Jones, A. K., Sikka, V. K., Wu, J. & Gao, D. Anti-Icing Superhydrophobic Coatings. *Langmuir* **25,** 12444–12448 (2009).

5. Leslie, D. C. *et al.* A bioinspired omniphobic surface coating on medical devices prevents thrombosis and biofouling. *Nat. Biotechnol.* **32,** 1134–1140 (2014).

6. Epstein, A. K., Wong, T.-S., Belisle, R. A., Boggs, E. M. & Aizenberg, J. Liquid-infused structured surfaces with exceptional anti-biofouling performance. *Proc. Natl. Acad. Sci.* **109,** 13182–13187 (2012).

7. Lafuma, A. & Quéré, D. Superhydrophobic states. *Nat. Mater.* **2,** 457–460 (2003).

8. Wenzel, R. N. RESISTANCE OF SOLID SURFACES TO WETTING BY WATER. *Ind. Eng. Chem.* **28,** 988–994 (1936).

9. Cassie, A. B. D. & Baxter, S. Wettability of porous surfaces. *Trans. Faraday Soc.* **40,** 546 (1944).

10. Nosonovsky, M. Multiscale Roughness and Stability of Superhydrophobic Biomimetic Interfaces. *Langmuir* **23,** 3157–3161 (2007).

11. Shirtcliffe, N. J., McHale, G., Newton, M. I., Chabrol, G. & Perry, C. C. Dual-Scale Roughness Produces Unusually Water-Repellent Surfaces. *Adv. Mater.* **16,** 1929–1932 (2004).

12. Lin, P.-C. & Yang, S. Mechanically switchable wetting on wrinkled elastomers with dual-scale roughness. *Soft Matter* **5,** 1011 (2009).

13. Kota, A. K., Kwon, G. & Tuteja, A. The design and applications of superomniphobic surfaces. *NPG Asia Mater.* **6,** e109–e109 (2014).

14. Hensel, R., Neinhuis, C. & Werner, C. The springtail cuticle as a blueprint for omniphobic surfaces. *Chem. Soc. Rev.* **45,** 323–341 (2016).

15. Wong, T.-S. *et al.* Bioinspired self-repairing slippery surfaces with pressure-stable omniphobicity. *Nature* **477,** 443–447 (2011).

16. Kim, P., Kreder, M. J., Alvarenga, J. & Aizenberg, J. Hierarchical or Not? Effect of the Length Scale and Hierarchy of the Surface Roughness on Omniphobicity of Lubricant-Infused Substrates. *Nano Lett.* **13,** 1793–1799 (2013).

17. Chu, Z. & Seeger, S. Superamphiphobic surfaces. *Chem Soc Rev* **43,** 2784–2798 (2014).

18. Zhu, P., Kong, T., Tang, X. & Wang, L. Well-defined porous membranes for robust omniphobic surfaces via microfluidic emulsion templating. *Nat. Commun.* **8,** 15823 (2017).

19. Tuteja, A., Choi, W., Mabry, J. M., McKinley, G. H. & Cohen, R. E. Robust omniphobic surfaces. *Proc. Natl. Acad. Sci.* **105,** 18200–18205 (2008).

20. Wu, W. *et al.* Alumina nanowire forests via unconventional anodization and super-repellency plus low adhesion to diverse liquids. *Chem. Commun.* 1043 (2009). doi:10.1039/b818633b

21. Mazumder, P. *et al.* Superomniphobic, Transparent, and Antireflection Surfaces Based on Hierarchical Nanostructures. *Nano Lett.* **14,** 4677–4681 (2014).

22. Gabardo, C. M., Yang, J., Smith, N. J., Adams-McGavin, R. C. & Soleymani, L. Programmable Wrinkling of Self-Assembled Nanoparticle Films on Shape Memory Polymers. *ACS Nano* **10,** 8829–8836 (2016).

23. Schauer, S., Worgull, M. & Hölscher, H. Bio-inspired hierarchical micro- and nano-wrinkles obtained via mechanically directed self-assembly on shape-memory polymers. *Soft Matter* **13,** 4328–4334 (2017).

24. Efimenko, K. *et al.* Nested self-similar wrinkling patterns in skins. *Nat. Mater.* **4,** 293–297 (2005).

25. Deng, X., Mammen, L., Butt, H.-J. & Vollmer, D. Candle Soot as a Template for a Transparent Robust Superamphiphobic Coating. *Science* **335,** 67–70 (2012).

26. Zhang, J. & Seeger, S. Superoleophobic Coatings with Ultralow Sliding Angles Based on Silicone Nanofilaments. *Angew. Chem. Int. Ed.* **50,** 6652–6656 (2011).

27. Hrncír, E. & Rosina, J. Surface tension of blood. *Physiol. Res.* **46,** 319–321 (1997).

28. Chen, K., Zhou, S. & Wu, L. Self-Healing Underwater Superoleophobic and Antibiofouling Coatings Based on the Assembly of Hierarchical Microgel Spheres. *ACS Nano* **10,** 1386–1394 (2016).

29. Scarratt, L. R. J., Hoatson, B. S., Wood, E. S., Hawkett, B. S. & Neto, C. Durable Superhydrophobic Surfaces via Spontaneous Wrinkling of Teflon AF. *ACS Appl. Mater. Interfaces* **8,** 6743–6750 (2016).

30. Rahmawan, Y., Moon, M.-W., Kim, K.-S., Lee, K.-R. & Suh, K.-Y. Wrinkled, Dual-Scale Structures of Diamond-Like Carbon (DLC) for Superhydrophobicity. *Langmuir* **26,** 484–491 (2010).

31. Zang, J. *et al.* Multifunctionality and control of the crumpling and unfolding of large-area graphene. *Nat. Mater.* **12,** 321–325 (2013).

32. Li, Y., Dai, S., John, J. & Carter, K. R. Superhydrophobic Surfaces from Hierarchically Structured Wrinkled Polymers. *ACS Appl. Mater. Interfaces* **5,** 11066–11073 (2013).

33. Sarwate, P., Chakraborty, A., Garg, V. & Luo, C. Controllable strain recovery of *shape memory* polystyrene to achieve superhydrophobicity with tunable adhesion. *J. Micromechanics Microengineering* **24,** 115006 (2014).

34. Lee, W.-K., Jung, W.-B., Nagel, S. R. & Odom, T. W. Stretchable Superhydrophobicity from Monolithic, Three-Dimensional Hierarchical Wrinkles. *Nano Lett.* **16,** 3774–3779 (2016).

35. Erasmus, E. & Barkhuysen, F. A. Superhydrophobic cotton by fluorosilane modification. *IJFTR Vol344 Dec. 2009* (2009).

36. Howarter, J. A. & Youngblood, J. P. Optimization of Silica Silanization by 3-Aminopropyltriethoxysilane. *Langmuir* **22,** 11142–11147 (2006).

37. Zihua, Z., Tao, Z. & Zhongfan, L. Raman scattering enhancement contributed from individual gold nanoparticles and interparticle coupling. *Nanotechnology* **15,** 357–364 (2004).

38. Paven, M. *et al.* Super liquid-repellent gas membranes for carbon dioxide capture and heart–lung machines. *Nat. Commun.* **4,** (2013).

39. Brown, P. S. & Bhushan, B. Bioinspired, roughness-induced, water and oil super-philic and super-phobic coatings prepared by adaptable layer-by-layer technique. *Sci. Rep.* **5,** (2015).

40. Wang, Y. & Bhushan, B. Wear-Resistant and Antismudge Superoleophobic Coating on Polyethylene Terephthalate Substrate Using SiO_2 Nanoparticles. *ACS Appl. Mater. Interfaces* **7,** 743–755 (2015).

41. Li, D. & Neumann, A. . Contact angles on hydrophobic solid surfaces and their interpretation. *J. Colloid Interface Sci.* **148,** 190–200 (1992).

42. Milne, A. J. B. & Amirfazli, A. The Cassie equation: How it is meant to be used. *Adv. Colloid Interface Sci.* **170,** 48–55 (2012).

43. Hideo Nakae, Ryuichi Inui, Yosuke Hirata & Hiroyuki Saito. Effects of surface roughness on wettability. *Acta Mater.* **46,** 2313–2318 (1998).

44. Yan, L., Wang, K., Wu, J. & Ye, L. Hydrophobicity of model surfaces with closely packed nano- and micro-spheres. *Colloids Surf. Physicochem. Eng. Asp.* **296,** 123–131 (2007).

45. Shiu, J.-Y., Kuo, C.-W., Chen, P. & Mou, C.-Y. Fabrication of Tunable Superhydrophobic Surfaces by Nanosphere Lithography. *Chem. Mater.* **16,** 561–564 (2004).

46. Herminghaus, S. Roughness-induced non-wetting. *EPL Europhys. Lett.* **52,** 165 (2000).

47. Marmur, A. From Hygrophilic to Superhygrophobic: Theoretical Conditions for Making High-Contact-Angle Surfaces from Low-Contact-Angle Materials. *Langmuir* **24,** 7573–7579 (2008).

48. Epstein, A. K., Pokroy, B., Seminara, A. & Aizenberg, J. Bacterial biofilm shows persistent resistance to liquid wetting and gas penetration. *Proc. Natl. Acad. Sci.* **108,** 995–1000 (2011).

49. Choi, W. *et al.* Fabrics with Tunable Oleophobicity. *Adv. Mater.* **21,** 2190–2195 (2009).

50. Barthlott, W. & Neinhuis, C. Purity of the sacred lotus, or escape from contamination in biological surfaces. *Planta* **202,** 1–8 (1997).

51. Ensikat, H. J., Ditsche-Kuru, P., Neinhuis, C. & Barthlott, W. Superhydrophobicity in perfection: the outstanding properties of the lotus leaf. *Beilstein J. Nanotechnol.* **2,** 152–161 (2011).

52. Greco, F. *et al.* Microwrinkled Conducting Polymer Interface for Anisotropic Multicellular Alignment. *ACS Appl. Mater. Interfaces* **5,** 573–584 (2013).

53. Gabardo, C. M., Zhu, Y., Soleymani, L. & Moran-Mirabal, J. M. Bench-Top Fabrication of Hierarchically Structured High-Surface-Area Electrodes. *Adv. Funct. Mater.* **23,** 3030–3039 (2013).

54. Adams-McGavin, R. C. *et al.* Nanoporous and wrinkled electrodes enhance the sensitivity of glucose biosensors. *Electrochimica Acta* **242,** 1–9 (2017).

55. Woo, S. M., Gabardo, C. M. & Soleymani, L. Prototyping of Wrinkled Nano-/Microstructured Electrodes for Electrochemical DNA Detection. *Anal. Chem.* **86,** 12341–12347 (2014).

56. Kim, J. B. *et al.* Wrinkles and deep folds as photonic structures in photovoltaics. *Nat. Photonics* **6,** 327–332 (2012).

57. Tenjimbayashi, M. *et al.* Droplet Motion Control on Dynamically Hydrophobic Patterned Surfaces as Multifunctional Liquid Manipulators. *ACS Appl. Mater. Interfaces* **9,** 10371–10377 (2017).

58. Grabar, K. C., Freeman, R. G., Hommer, M. B. & Natan, M. J. Preparation and Characterization of Au Colloid Monolayers. *Anal. Chem.* **67,** 735–743 (1995).

59. Shillingford, C., MacCallum, N., Wong, T.-S., Kim, P. & Aizenberg, J. Fabrics coated with lubricated nanostructures display robust omniphobicity. *Nanotechnology* **25,** 014019 (2014).

Chapter 4

Conclusion

4.1 Thesis summary

In this work, we had developed fast and easy processes for creating wrinkled structures for use in stretchable electrodes and in hierarchical surfaces. We investigated the potential of wrinkled gold as a stretchable electrode for electrochemical sensing. The potential of wrinkles as part of a hierarchical structure for omniphobicity was investigated by fabricating surfaces that are just wrinkles, just nanoparticles or wrinkles with nanoparticles.

The stretchable electrodes' morphology with and without strain was characterised through SEM imaging. The electrodes' performances were examined through electrochemical tests (for electroactive surface area and glucose concentration detection) and resistivity measurements of the electrodes with and without strain. Through analysis of the results, it was shown that wrinkled gold electrode transferred onto Ecoflex works well for enzyme-free glucose sensing under strain.

For structured surfaces fabricated for omniphobicity tests, the morphologies were investigated through SEM imaging. Wettability of the surfaces were characterised through contact angle measurements for water and lower surface tension liquid. Adhesion of the hierarchical surfaces were tested through sliding angle measurement. Viability of the surfaces for medical devices were examined through blood contact angle and adhesion test.

The results demonstrated that it is viable to use wrinkle with nanoparticles for creation of hierarchical surfaces that are omniphobic.

4.2 Thesis conclusion

In chapter 2, it was reported that there were slight differences in the morphology of electrode before and after transfer but the electrochemical sensitivity (measured using external electrodes) of the stretchable electrode (860 ± 60 µA/mM.cm^2) is comparable to electrode before transfer (710 ± 30 µA/mM.cm^2). By consolidating the electrochemical electrodes onto the substrates, a sensitivity that is comparable to previous values were determined (730 ± 80 µA/mM.cm^2). The electroactive surface area was shown to be consistent up to 45% strain.

The stretchable electrodes fabricated have comparable sheet resistance with the electrodes before transfer. In addition, the relative resistance of the electrodes in relation to strain was measured. The resistance measured demonstrated that the stretchable electrode work well up to 30% strain. The electrode configuration was also shown to matter as it works better when the current is travelling parallel to the strain compared to when the current is travelling perpendicular to strain.

In chapter 3, it was shown that we had successfully fabricated surfaces with different structures. It was reported that hierarchical structures with both wrinkles and nanoparticles are effective for creating surfaces that are omniphobic. The fluorinated surfaces with wrinkles, nanoparticles and wrinkles with nanoparticles were all shown to be hydrophobic, with water contact angle ranging from 125° to 155°. However, for low surface tension liquid, the surfaces with just wrinkles or nanoparticles were oleophilic with hexadecane contact angle of less than 75°.

The combination of both structures resulted in an oleophobic surface, with hexadecane contact angle of more than 110°. The results demonstrated that the hierarchical structures were omniphobic. These omniphobic surfaces were also shown to be repellent to blood (>135°), with 90% less adhesion compared to untreated surfaces, demonstrating the potential of such surfaces for medical devices.

4.3 Contribution to the field

4.3.1 Simple fabrication method

The processes for both stretchable electrodes and omniphobic surfaces take just a few days and can be done in batches of more than ten samples in a laboratory set-up. As the fabrication method is solution based with many samples being able to be treated in parallel, it can be scaled up as a high throughput industrial manufacturing process.

The equipment required in these processes are easily found bench-top instruments with easily controlled and achievable parameters. The use of UVO treatment on polystyrene provides an easy way to achieve wrinkles on the surface and the activated surfaces, consisting of hydroxyl groups, also allow easy deposition of coating.

As can be seen from Table 1.2, the use of wrinkling is one of the least complex fabrication methods for stretchable glucose sensors, compared to other methods [54,56,58]: photolithography, electron beam evaporation or chemical vapour deposition. Similarly, for hierarchical structures, wrinkling is a competitive fabrication method compared to electrochemical [88] or reactive ion [90] etching, photolithography [72] or electrospinning [72].

4.3.2 Stretchable non-enzymatic glucose electrodes

As can be seen from the motivation section, there are still few papers studying non-enzymatic detection of glucose on stretchable electrode. A previous paper [55] had investigated the use carbon nanotube layers on gold nanosheets as a stretchable electrode for non-enzymatic glucose sensing, usable up to 30% strain with 10.89 μA/mMcm^2 (0.05-0.3 mM) sensitivity in neutral solution.

In our work, we achieved a much higher sensitivity 860 (external reference and counter electrodes) or 730 μA/mMcm^2 (on chip electrochemical cell) (1-10 mM) in basic solution. Even though the results in this work are done in basic solution and with pulsed amperometric rather than the usual amperometric, we see from studies [53] that electrodes with sensitivity of 222 μA/mMcm^2 in basic solution have sensitivity of 38 μA/mMcm^2 in neutral solution. This supports the supposition that our work had achieved a stretchable electrode of higher sensitivity than the previous paper for glucose detection. The strain achieved in our electrode is 30%, similar with the paper.

4.3.3 Omniphobic surfaces

Previous literature reported surfaces achieving water contact angle of 172° [23] and hexadecane contact angle of 174° [93]. For wrinkled surfaces fabricated from buckling of surfaces, there were no studies done on repellence of oil. Few works had also been done on combination of structures.

In our work, we have shown that hierarchical structures with wrinkles and nanoparticles surfaces achieved water contact angle of more than 150°, sliding angle of less than 20° and hexadecane contact angle of more than 110°. These contact angles are lower than what was shown in previous studies. However, by studying combination of structures involving wrinkles and nanoparticles for high and low surface tension liquid, we have demonstrated that wrinkles with nanoparticles surfaces are omniphobic. Nanoparticles are also shown to be more effective for oil repellence (~55°) compared to wrinkled structures (~26°). In addition, these omniphobic surfaces are also repellent to blood and have reduced blood adhesion and hence, have potential use in medical devices.

4.4 Future work

In this thesis, the focus was specifically on two areas, stretchability and omniphobicity of wrinkled structures. To further expand on these two areas, there are improvements that can be made as well as applications that can be explored.

The development of stretchable electrode as a wearable sensor to detect glucose in sweat or blood can be improved by investigating ways to lower the detection range tested for glucose sensing to show its viability of glucose in sweat testing (0.01 to 0.7 mM [56]). Electronic components such as integrated circuits to control the potential provided and recorded from the electrodes can be incorporated. The device can be tested on the skin of people working out or tested with blood of people with diabetes.

Nanoporous wrinkled structure can be investigated for stretchable electrode as it had been shown to increase sensitivity for glucose detection [53]. There are two possible strategies to achieve this, through etching of the transferred electrodes or transfer of nanoporous electrodes.

The hierarchical surfaces can be improved to achieve superomniphobic surfaces. This can be done through investigating the deposition of nanoparticles of different shape or varying the wrinkle wavelength/amplitude through changing the UVO treatment duration. These omniphobic surface can also be used for patterning of target areas for fluid deposition which may be helpful for biosensor development.

Biofouling, in terms of bacterial contamination leading to biofilm formation on medical devices is a big issue as microbial biofilm can be linked to over 80% of human infections [125]. Hence, the investigation of whether omniphobic surfaces would work to inhibit the growth or adhesion of bacterial contamination would have great implication for medical devices.

It had been shown that aquatic devices can be made from superhydrophobic material to achieve buoyancy [126]. The fabricated omniphobic surfaces can be tested to see if it could be used as part of miniature robotic aquatic devices for buoyancy and if it would be able to withstand fouling such as oil contamination.

In addition to the above, fundamental studies can also be done to enhance understanding into the buckling of surface by investigating the effect of having different soft molecular layers on the wrinkles created on shrunken UVO treated polystyrene. With such a study, further insights may be provided on the basic buckling theoretical models mentioned in the introduction.

Chapter 5 Bibliography

1. Bowden, N., Brittain, S., Evans, A. G., Hutchinson, J. W. & Whitesides, G. M. Spontaneous formation of ordered structures in thin films of metals supported on an elastomeric polymer. *Nature* **393,** 146 (1998).

2. Kim, P., Abkarian, M. & Stone, H. A. Hierarchical folding of elastic membranes under biaxial compressive stress. *Nat. Mater.* **10,** 952–957 (2011).

3. Sarwate, P., Chakraborty, A., Garg, V. & Luo, C. Controllable strain recovery of *shape memory* polystyrene to achieve superhydrophobicity with tunable adhesion. *J. Micromechanics Microengineering* **24,** 115006 (2014).

4. Nania, M., Foglia, F., Matar, O. K. & Cabral, J. T. Sub-100 nm wrinkling of polydimethylsiloxane by double frontal oxidation. *Nanoscale* **9,** 2030–2037 (2017).

5. Chandra, D., Yang, S. & Lin, P.-C. Strain responsive concave and convex microlens arrays. *Appl. Phys. Lett.* **91,** 251912 (2007).

6. Xia, Y., Rogers, J. A., Paul, K. E. & Whitesides, G. M. Unconventional Methods for Fabricating and Patterning Nanostructures. *Chem. Rev.* **99,** 1823–1848 (1999).

7. Kumar, A., Abbott, N. L., Biebuyck, H. A., Kim, E. & Whitesides, G. M. Patterned Self-Assembled Monolayers and Meso-Scale Phenomena. *Acc. Chem. Res.* **28,** 219–226 (1995).

8. *Size Effects in Nanostructures*. **205,** (Springer Berlin Heidelberg, 2014).
9. Reed, M. A. Quantum Dots. *Sci. Am.* **268,** 118–123 (1993).
10. Likharev, K. K. Correlated discrete transfer of single electrons in ultrasmall tunnel junctions. *IBM J. Res. Dev.* **32,** 144–158 (1988).
11. Betzig, E. & Trautman, J. K. Near-Field Optics: Microscopy, Spectroscopy, and Surface Modification Beyond the Diffraction Limit. *Science* **257,** 189–195 (1992).
12. Park, S., Chung, T. D. & Kim, H. C. Nonenzymatic Glucose Detection Using Mesoporous Platinum. *Anal. Chem.* **75,** 3046–3049 (2003).
13. Gabardo, C. M., Yang, J., Smith, N. J., Adams-McGavin, R. C. & Soleymani, L. Programmable Wrinkling of Self-Assembled Nanoparticle Films on Shape Memory Polymers. *ACS Nano* **10,** 8829–8836 (2016).
14. Schauer, S., Worgull, M. & Hölscher, H. Bio-inspired hierarchical micro- and nano-wrinkles obtained via mechanically directed self-assembly on shape-memory polymers. *Soft Matter* **13,** 4328–4334 (2017).
15. Efimenko, K. *et al.* Nested self-similar wrinkling patterns in skins. *Nat. Mater.* **4,** 293–297 (2005).

16. Allen, H. G. WRINKLING AND OTHER FORMS OF LOCAL INSTABILITY. in *Analysis and Design of Structural Sandwich Panels* 156–189 (Elsevier, 1969). doi:10.1016/B978-0-08-012870-2.50012-2

17. Stafford, C. M. *et al.* A buckling-based metrology for measuring the elastic moduli of polymeric thin films. *Nat. Mater.* **3,** 545–550 (2004).

18. Gill, U. *et al.* Beyond buckling: humidity-independent measurement of the mechanical properties of green nanobiocomposite films. *Nanoscale* **9,** 7781–7790 (2017).

19. Gabardo, C. M., Zhu, Y., Soleymani, L. & Moran-Mirabal, J. M. Bench-Top Fabrication of Hierarchically Structured High-Surface-Area Electrodes. *Adv. Funct. Mater.* **23,** 3030–3039 (2013).

20. Adams-McGavin, R. C. *et al.* Nanoporous and wrinkled electrodes enhance the sensitivity of glucose biosensors. *Electrochimica Acta* **242,** 1–9 (2017).

21. Woo, S. M., Gabardo, C. M. & Soleymani, L. Prototyping of Wrinkled Nano-/Microstructured Electrodes for Electrochemical DNA Detection. *Anal. Chem.* **86,** 12341–12347 (2014).

22. Kim, J. B. *et al.* Wrinkles and deep folds as photonic structures in photovoltaics. *Nat. Photonics* **6,** 327–332 (2012).

23. Scarratt, L. R. J., Hoatson, B. S., Wood, E. S., Hawkett, B. S. & Neto, C. Durable Superhydrophobic Surfaces via Spontaneous Wrinkling of Teflon AF. *ACS Appl. Mater. Interfaces* **8,** 6743–6750 (2016).

24. Rahmawan, Y., Moon, M.-W., Kim, K.-S., Lee, K.-R. & Suh, K.-Y. Wrinkled, Dual-Scale Structures of Diamond-Like Carbon (DLC) for Superhydrophobicity. *Langmuir* **26,** 484–491 (2010).

25. Zang, J. *et al.* Multifunctionality and control of the crumpling and unfolding of large-area graphene. *Nat. Mater.* **12,** 321–325 (2013).

26. Li, Y., Dai, S., John, J. & Carter, K. R. Superhydrophobic Surfaces from Hierarchically Structured Wrinkled Polymers. *ACS Appl. Mater. Interfaces* **5,** 11066–11073 (2013).

27. Lee, S. G. *et al.* Switchable Transparency and Wetting of Elastomeric Smart Windows. *Adv. Mater.* **22,** 5013–5017 (2010).

28. Lin, P.-C. & Yang, S. Mechanically switchable wetting on wrinkled elastomers with dual-scale roughness. *Soft Matter* **5,** 1011 (2009).

29. Chung, J. Y., Youngblood, J. P. & Stafford, C. M. Anisotropic wetting on tunable micro-wrinkled surfaces. *Soft Matter* **3,** 1163 (2007).

30. Xia, D., Johnson, L. M. & López, G. P. Anisotropic Wetting Surfaces with One-Dimesional and Directional Structures: Fabrication Approaches, Wetting Properties and Potential Applications. *Adv. Mater.* **24,** 1287–1302 (2012).

31. Zhu, Y. & Moran-Mirabal, J. Highly Bendable and Stretchable Electrodes Based on Micro/Nanostructured Gold Films for Flexible Sensors and Electronics. *Adv. Electron. Mater.* **2,** 1500345 (2016).

32. Park, S.-J., Kim, J., Chu, M. & Khine, M. Highly Flexible Wrinkled Carbon Nanotube Thin Film Strain Sensor to Monitor Human Movement. *Adv. Mater. Technol.* **1,** 1600053 (2016).

33. Kim, J. *et al.* Highly stretchable wrinkled gold thin film wires. *Appl. Phys. Lett.* **108,** 061901 (2016).

34. Tang, J. *et al.* Highly Stretchable Electrodes on Wrinkled Polydimethylsiloxane Substrates. *Sci. Rep.* **5,** (2015).

35. Chae, S. H. *et al.* Transferred wrinkled Al2O3 for highly stretchable and transparent graphene–carbon nanotube transistors. *Nat. Mater.* **12,** 403–409 (2013).

36. Lipomi, D. J., Tee, B. C.-K., Vosgueritchian, M. & Bao, Z. Stretchable Organic Solar Cells. *Adv. Mater.* **23,** 1771–1775 (2011).

37. Greco, F. *et al.* Microwrinkled Conducting Polymer Interface for Anisotropic Multicellular Alignment. *ACS Appl. Mater. Interfaces* **5,** 573–584 (2013).

38. Nathan, D. M. Diabetes: Advances in Diagnosis and Treatment. *JAMA* **314,** 1052 (2015).

39. Moyer, J., Wilson, D., Finkelshtein, I., Wong, B. & Potts, R. Correlation Between Sweat Glucose and Blood Glucose in Subjects with Diabetes. *Diabetes Technol. Ther.* **14,** 398–402 (2012).

40. Windmiller, J. R. *et al.* Electrochemical sensing based on printable temporary transfer tattoos. *Chem. Commun.* **48,** 6794 (2012).

41. Zhao, S. *et al.* Recent Advancements in Flexible and Stretchable Electrodes for Electromechanical Sensors: Strategies, Materials, and Features. *ACS Appl. Mater. Interfaces* **9,** 12147–12164 (2017).

42. Rogers, J. A., Someya, T. & Huang, Y. Materials and Mechanics for Stretchable Electronics. *Science* **327,** 1603–1607 (2010).

43. Yoon, Y. *et al.* Highly Stretchable and Conductive Silver Nanoparticle Embedded Graphene Flake Electrode Prepared by In situ Dual Reduction Reaction. *Sci. Rep.* **5,** (2015).

44. Yao, S. & Zhu, Y. Wearable multifunctional sensors using printed stretchable conductors made of silver nanowires. *Nanoscale* **6,** 2345 (2014).

45. Lee, S.-K. *et al.* Stretchable Graphene Transistors with Printed Dielectrics and Gate Electrodes. *Nano Lett.* **11,** 4642–4646 (2011).

46. Zhang, H. *et al.* Piezoresistive Sensor with High Elasticity Based on 3D Hybrid Network of Sponge@CNTs@Ag NPs. *ACS Appl. Mater. Interfaces* **8,** 22374–22381 (2016).

47. Mu, J. *et al.* An Elastic Transparent Conductor Based on Hierarchically Wrinkled Reduced Graphene Oxide for Artificial Muscles and Sensors. *Adv. Mater.* **28,** 9491–9497 (2016).

48. Xu, F., Lu, W. & Zhu, Y. Controlled 3D Buckling of Silicon Nanowires for Stretchable Electronics. *ACS Nano* **5,** 672–678 (2011).

49. Yu, Y. *et al.* Three-Dimensional Compressible and Stretchable Conductive Composites. *Adv. Mater.* **26,** 810–815 (2014).

50. Li, X. *et al.* Multifunctional graphene woven fabrics. *Sci. Rep.* **2,** (2012).

51. Park, S., Boo, H. & Chung, T. D. Electrochemical non-enzymatic glucose sensors. *Anal. Chim. Acta* **556,** 46–57 (2006).

52. Song, Y.-Y., Zhang, D., Gao, W. & Xia, X.-H. Nonenzymatic Glucose Detection by Using a Three-Dimensionally Ordered, Macroporous Platinum Template. *Chem. - Eur. J.* **11,** 2177–2182 (2005).

53. Adams-McGavin, R. C. *et al.* Nanoporous and wrinkled electrodes enhance the sensitivity of glucose biosensors. *Electrochimica Acta* **242,** 1–9 (2017).

54. Gao, W. *et al.* Fully integrated wearable sensor arrays for multiplexed in situ perspiration analysis. *Nature* **529,** 509–514 (2016).

55. Oh, S. Y. *et al.* Skin-Attachable, Stretchable Electrochemical Sweat Sensor for Glucose and pH Detection. *ACS Appl. Mater. Interfaces* **10,** 13729–13740 (2018).

56. Lee, H. *et al.* A graphene-based electrochemical device with thermoresponsive microneedles for diabetes monitoring and therapy. *Nat. Nanotechnol.* **11,** 566–572 (2016).

57. Bandodkar, A. J. *et al.* Tattoo-Based Noninvasive Glucose Monitoring: A Proof-of-Concept Study. *Anal. Chem.* **87,** 394–398 (2015).

58. You, X. & Pak, J. J. Graphene-based field effect transistor enzymatic glucose biosensor using silk protein for enzyme immobilization and device substrate. *Sens. Actuators B Chem.* **202,** 1357–1365 (2014).

59. Fürstner, R., Barthlott, W., Neinhuis, C. & Walzel, P. Wetting and Self-Cleaning Properties of Artificial Superhydrophobic Surfaces. *Langmuir* **21,** 956–961 (2005).

60. Parkin, I. P. & Palgrave, R. G. Self-cleaning coatings. *J. Mater. Chem.* **15,** 1689 (2005).

61. Wang, Y., Xue, J., Wang, Q., Chen, Q. & Ding, J. Verification of Icephobic/Anti-icing Properties of a Superhydrophobic Surface. *ACS Appl. Mater. Interfaces* **5,** 3370–3381 (2013).

62. Cao, L., Jones, A. K., Sikka, V. K., Wu, J. & Gao, D. Anti-Icing Superhydrophobic Coatings. *Langmuir* **25,** 12444–12448 (2009).

63. Leslie, D. C. *et al.* A bioinspired omniphobic surface coating on medical devices prevents thrombosis and biofouling. *Nat. Biotechnol.* **32,** 1134–1140 (2014).

64. Epstein, A. K., Wong, T.-S., Belisle, R. A., Boggs, E. M. & Aizenberg, J. Liquid-infused structured surfaces with exceptional anti-biofouling performance. *Proc. Natl. Acad. Sci.* **109,** 13182–13187 (2012).

65. Glavan, A. C. *et al.* Omniphobic "R ^{F} Paper" Produced by Silanization of Paper with Fluoroalkyltrichlorosilanes. *Adv. Funct. Mater.* **24,** 60–70 (2014).

66. Vashist, S. Point-of-Care Diagnostics: Recent Advances and Trends. *Biosensors* **7,** 62 (2017).

67. Lafuma, A. & Quéré, D. Superhydrophobic states. *Nat. Mater.* **2,** 457–460 (2003).

68. Wenzel, R. N. RESISTANCE OF SOLID SURFACES TO WETTING BY WATER. *Ind. Eng. Chem.* **28,** 988–994 (1936).

69. Cassie, A. B. D. & Baxter, S. Wettability of porous surfaces. *Trans. Faraday Soc.* **40,** 546 (1944).

70. Nosonovsky, M. Multiscale Roughness and Stability of Superhydrophobic Biomimetic Interfaces. *Langmuir* **23,** 3157–3161 (2007).

71. Shirtcliffe, N. J., McHale, G., Newton, M. I., Chabrol, G. & Perry, C. C. Dual-Scale Roughness Produces Unusually Water-Repellent Surfaces. *Adv. Mater.* **16,** 1929–1932 (2004).

72. Tuteja, A., Choi, W., Mabry, J. M., McKinley, G. H. & Cohen, R. E. Robust omniphobic surfaces. *Proc. Natl. Acad. Sci.* **105,** 18200–18205 (2008).

73. Tuteja, A. *et al.* Designing Superoleophobic Surfaces. *Science* **318,** 1618–1622 (2007).

74. Hrncír, E. & Rosina, J. Surface tension of blood. *Physiol. Res.* **46,** 319–321 (1997).

75. Chen, K., Zhou, S. & Wu, L. Self-Healing Underwater Superoleophobic and Antibiofouling Coatings Based on the Assembly of Hierarchical Microgel Spheres. *ACS Nano* **10,** 1386–1394 (2016).

76. El Fray, M., Prowans, P., Puskas, J. E. & Altstädt, V. Biocompatibility and Fatigue Properties of Polystyrene−Polyisobutylene−Polystyrene, an Emerging Thermoplastic Elastomeric Biomaterial. *Biomacromolecules* **7,** 844–850 (2006).

77. Mabry, J. M., Vij, A., Iacono, S. T. & Viers, B. D. Fluorinated Polyhedral Oligomeric Silsesquioxanes (F-POSS). *Angew. Chem. Int. Ed.* **47,** 4137–4140 (2008).

78. Boban, M. *et al.* Smooth, All-Solid, Low-Hysteresis, Omniphobic Surfaces with Enhanced Mechanical Durability. *ACS Appl. Mater. Interfaces* **10,** 11406–11413 (2018).

79. Liu, P. *et al.* Development of “Liquid-like” Copolymer Nanocoatings for Reactive Oil-Repellent Surface. *ACS Nano* **11,** 2248–2256 (2017).

80. Tenjimbayashi, M. *et al.* Droplet Motion Control on Dynamically Hydrophobic Patterned Surfaces as Multifunctional Liquid Manipulators. *ACS Appl. Mater. Interfaces* **9,** 10371–10377 (2017).

81. Yuan, Y., Hays, M. P., Hardwidge, P. R. & Kim, J. Surface characteristics influencing bacterial adhesion to polymeric substrates. *RSC Adv.* **7,** 14254–14261 (2017).

82. Zhu, P., Kong, T., Tang, X. & Wang, L. Well-defined porous membranes for robust omniphobic surfaces via microfluidic emulsion templating. *Nat. Commun.* **8,** 15823 (2017).

83. Chakraborty, A., Xiang, M. & Luo, C. Fabrication of Super-Hydrophobic Microchannels via Strain-Recovery Deformations of Polystyrene and Oxygen Reactive Ion Etch. *Materials* **6,** 3610–3623 (2013).

84. Dramé, A., Darmanin, T., Dieng, S. Y., Taffin de Givenchy, E. & Guittard, F. Superhydrophobic and oleophobic surfaces containing wrinkles and nanoparticles of PEDOT with two short fluorinated chains. *RSC Adv.* **4,** 10935 (2014).

85. Paven, M. *et al.* Super liquid-repellent gas membranes for carbon dioxide capture and heart–lung machines. *Nat. Commun.* **4,** (2013).

86. Qu, M. *et al.* Facile Selective and Diverse Fabrication of Superhydrophobic, Superoleophobic-Superhydrophilic and Superamphiphobic Materials from Kaolin. *ACS Appl. Mater. Interfaces* **9,** 1011–1020 (2017).

87. Sriramulu, D., Reed, E. L., Annamalai, M., Venkatesan, T. V. & Valiyaveettil, S. Synthesis and Characterization of Superhydrophobic, Self-cleaning NIR-reflective Silica Nanoparticles. *Sci. Rep.* **6,** (2016).

88. Wu, W. *et al.* Alumina nanowire forests via unconventional anodization and super-repellency plus low adhesion to diverse liquids. *Chem. Commun.* 1043 (2009). doi:10.1039/b818633b

89. Deng, X., Mammen, L., Butt, H.-J. & Vollmer, D. Candle Soot as a Template for a Transparent Robust Superamphiphobic Coating. *Science* **335,** 67–70 (2012).

90. Mazumder, P. *et al.* Superomniphobic, Transparent, and Antireflection Surfaces Based on Hierarchical Nanostructures. *Nano Lett.* **14,** 4677–4681 (2014).

91. Brown, P. S. & Bhushan, B. Bioinspired, roughness-induced, water and oil super-philic and super-phobic coatings prepared by adaptable layer-by-layer technique. *Sci. Rep.* **5,** (2015).

92. Wang, Y. & Bhushan, B. Wear-Resistant and Antismudge Superoleophobic Coating on Polyethylene Terephthalate Substrate Using SiO_2 Nanoparticles. *ACS Appl. Mater. Interfaces* **7,** 743–755 (2015).

93. Zhang, J. & Seeger, S. Superoleophobic Coatings with Ultralow Sliding Angles Based on Silicone Nanofilaments. *Angew. Chem. Int. Ed.* **50,** 6652–6656 (2011).

94. Gabardo, C. M. *et al.* Rapid prototyping of all-solution-processed multi-lengthscale electrodes using polymer-induced thin film wrinkling. *Sci. Rep.* **7,** 42543 (2017).

95. Auguste, A., Jin, L., Suo, Z. & Hayward, R. C. The role of substrate pre-stretch in post-wrinkling bifurcations. *Soft Matter* **10,** 6520 (2014).

96. Park, H.-G., Jeong, H.-C., Jung, Y. H. & Seo, D.-S. Control of the wrinkle structure on surface-reformed poly(dimethylsiloxane) via ion-beam bombardment. *Sci. Rep.* **5,** (2015).

97. Chung, J. Y., Nolte, A. J. & Stafford, C. M. Diffusion-Controlled, Self-Organized Growth of Symmetric Wrinkling Patterns. *Adv. Mater.* **21,** 1358–1362 (2009).

98. Torres, J. M., Stafford, C. M. & Vogt, B. D. Manipulation of the Elastic Modulus of Polymers at the Nanoscale: Influence of UV−Ozone Cross-Linking and Plasticizer. *ACS Nano* **4,** 5357–5365 (2010).

99. Volynskii, A. L., Bazhenov, S., Lebedeva, O. V. & Bakeev, N. F. Mechanical buckling instability of thin coatings deposited on soft polymer substrates. *J. Mater. Sci.* **35,** 547–554 (2000).

100. Chung, J. Y., Nolte, A. J. & Stafford, C. M. Surface Wrinkling: A Versatile Platform for Measuring Thin-Film Properties. *Adv. Mater.* **23,** 349–368 (2011).

101. Groenewold, J. Wrinkling of plates coupled with soft elastic media. *Phys. Stat. Mech. Its Appl.* **298,** 32–45 (2001).

102. Nolte, A. J., Cohen, R. E. & Rubner, M. F. A Two-Plate Buckling Technique for Thin Film Modulus Measurements: Applications to Polyelectrolyte Multilayers. *Macromolecules* **39,** 4841–4847 (2006).

103. Gaillard, J. G., Hendrus, C. & Vogt, B. D. Tunable Wrinkle and Crease Surface Morphologies from Photoinitiated Polymerization of Furfuryl Alcohol. *Langmuir* **29,** 15083–15089 (2013).

104. Watanabe, M. & Mizukami, K. Well-Ordered Wrinkling Patterns on Chemically Oxidized Poly(dimethylsiloxane) Surfaces. *Macromolecules* **45,** 7128–7134 (2012).

105. Khang, D.-Y., Rogers, J. A. & Lee, H. H. Mechanical Buckling: Mechanics, Metrology, and Stretchable Electronics. *Adv. Funct. Mater.* **19,** 1526–1536 (2009).

106. Jiang, H. *et al.* Finite deformation mechanics in buckled thin films on compliant supports. *Proc. Natl. Acad. Sci.* **104,** 15607–15612 (2007).

107. Elgrishi, N. *et al.* A Practical Beginner's Guide to Cyclic Voltammetry. *J. Chem. Educ.* **95,** 197–206 (2018).

108. Fischer, L. M. *et al.* Gold cleaning methods for electrochemical detection applications. *Microelectron. Eng.* **86,** 1282–1285 (2009).

109. Kahlert, H. Reference Electrodes. in *Electroanalytical Methods* (eds. Scholz, F. et al.) 291–308 (Springer Berlin Heidelberg, 2010). doi:10.1007/978-3-642-02915-8_15

110. Warsaw University, Department of Chemistry, Pasteura 1, 02-093 Warsaw, Poland & Łukaszewski, M. Electrochemical Methods of Real Surface Area Determination of Noble Metal Electrodes – an Overview. *Int. J. Electrochem. Sci.* 4442–4469 (2016). doi:10.20964/2016.06.71

111. Rouya, E., Cattarin, S., Reed, M. L., Kelly, R. G. & Zangari, G. Electrochemical Characterization of the Surface Area of Nanoporous Gold Films. *J. Electrochem. Soc.* **159,** K97–K102 (2012).

112. Tremiliosi-Filho, G., Dall'Antonia, L. H. & Jerkiewicz, G. Growth of surface oxides on gold electrodes under well-defined potential, time and temperature conditions. *J. Electroanal. Chem.* **578,** 1–8 (2005).

113. Hwang, D.-W., Lee, S., Seo, M. & Chung, T. D. Recent advances in electrochemical non-enzymatic glucose sensors – A review. *Anal. Chim. Acta* **1033,** 1–34 (2018).

114. Miccoli, I., Edler, F., Pfnür, H. & Tegenkamp, C. The 100th anniversary of the four-point probe technique: the role of probe geometries in isotropic and anisotropic systems. *J. Phys. Condens. Matter* **27,** 223201 (2015).

115. Becker, H. & Schnabl, R. Gold contact resistance: A microprocessor-controlled measurement system. *Gold Bull.* **15,** 78–80 (1982).

116. Young, T. An Essay on the Cohesion of Fluids. *Philos. Trans. R. Soc. Lond.* **95,** 65–87 (1805).

117. Law, K.-Y. & Zhao, H. *Surface Wetting*. (Springer International Publishing, 2016). doi:10.1007/978-3-319-25214-8

118. Chen, J., J. Hanson, B., A. Pasquinelli, M. & Fiber and Polymer Science, North Carolina State University, 2401 Research Drive, Raleigh, NC 27695, USA. Molecular Dynamics Simulations for Predicting Surface Wetting. *AIMS Mater. Sci.* **1,** 121–131 (2014).

119. Kota, A. K., Kwon, G. & Tuteja, A. The design and applications of superomniphobic surfaces. *NPG Asia Mater.* **6,** e109–e109 (2014).

120. Chu, Z. & Seeger, S. Superamphiphobic surfaces. *Chem Soc Rev* **43,** 2784–2798 (2014).

121. Genzer, J. & Efimenko, K. Creating Long-Lived Superhydrophobic Polymer Surfaces Through Mechanically Assembled Monolayers. *Science* **290,** 2130–2133 (2000).

122. Milne, A. J. B. & Amirfazli, A. The Cassie equation: How it is meant to be used. *Adv. Colloid Interface Sci.* **170,** 48–55 (2012).

123. Herminghaus, S. Roughness-induced non-wetting. *EPL Europhys. Lett.* **52,** 165 (2000).

124. Law, K.-Y. & Zhao, H. What Do Contact Angles Measure? in *Surface Wetting* 99–121 (Springer International Publishing, 2016). doi:10.1007/978-3-319-25214-8_5

125. Romero, R. *et al.* Detection of a microbial biofilm in intraamniotic infection. *Am. J. Obstet. Gynecol.* **198,** 135.e1-135.e5 (2008).

126. Zhang, X. *et al.* Bioinspired Aquatic Microrobot Capable of Walking on Water Surface Like a Water Strider. *ACS Appl. Mater. Interfaces* **3,** 2630–2636 (2011).